Cell Reports
Report

OPEN ACCESS
CellPress

Isolation and Molecular Characterization of Circulating Melanoma Cells

Xi Luo,[1,10] Devarati Mitra,[2] Ryan J. Sullivan,[1,3] Ben S. Wittner,[1] Anya M. Kimura,[1] Shiwei Pan,[1] Mai P. Hoang,[4] Brian W. Brannigan,[1] Donald P. Lawrence,[1,3] Keith T. Flaherty,[1,3] Lecia V. Sequist,[1,3] Martin McMahon,[5] Marcus W. Bosenberg,[6] Shannon L. Stott,[1,3,7] David T. Ting,[1,3] Sridhar Ramaswamy,[1,3] Mehmet Toner,[7,9] David E. Fisher,[1,2,8] Shyamala Maheswaran,[1,9,*] and Daniel A. Haber[1,3,10,*]

[1]Massachusetts General Hospital Cancer Center, Harvard Medical School, Charlestown, MA 02129, USA
[2]Cutaneous Biology Research Center, Massachusetts General Hospital, Charlestown, MA 02129, USA
[3]Department of Medicine, Massachusetts General Hospital and Harvard Medical School, Boston, MA 02114, USA
[4]Department of Pathology, Massachusetts General Hospital and Harvard Medical School, Boston, MA 02114, USA
[5]Helen Diller Family Comprehensive Cancer Center, University of California, San Francisco, San Francisco, CA 94143, USA
[6]Department of Dermatology, Yale University School of Medicine, New Haven, CT 06520, USA
[7]Center for Engineering in Medicine, Massachusetts General Hospital, Charlestown, MA 02129, USA
[8]Department of Dermatology, Massachusetts General Hospital and Harvard Medical School, Boston, MA 02114, USA
[9]Department of Surgery, Massachusetts General Hospital and Harvard Medical School, Boston, MA 02114, USA
[10]Howard Hughes Medical Institute, Bethesda, MD 20815, USA
*Correspondence: maheswaran@helix.mgh.harvard.edu (S.M.), haber@helix.mgh.harvard.edu (D.A.H.)
http://dx.doi.org/10.1016/j.celrep.2014.03.039
This is an open access article under the CC BY-NC-ND license (http://creativecommons.org/licenses/by-nc-nd/3.0/).

SUMMARY

Melanoma is an invasive malignancy with a high frequency of blood-borne metastases, but circulating tumor cells (CTCs) have not been readily isolated. We adapted microfluidic CTC capture to a tamoxifen-driven B-RAF/PTEN mouse melanoma model. CTCs were detected in all tumor-bearing mice and rapidly declined after B-RAF inhibitor treatment. CTCs were shed early from localized tumors, and a short course of B-RAF inhibition following surgical resection was sufficient to dramatically suppress distant metastases. The large number of CTCs in melanoma-bearing mice enabled a comparison of RNA-sequencing profiles with matched primary tumors. A mouse melanoma CTC-derived signature correlated with invasiveness and cellular motility in human melanoma. CTCs were detected in smaller numbers in patients with metastatic melanoma and declined with successful B-RAF-targeted therapy. Together, the capture and molecular characterization of CTCs provide insight into the hematogenous spread of melanoma.

INTRODUCTION

Recent advances in the treatment of metastatic melanoma have altered the outlook in this previously refractory cancer. In patients with metastatic B-RAF mutant melanoma, dramatic (albeit transient) responses to B-RAF-MAPK blockade require timely monitoring of drug response so that treatment options can be adjusted (Flaherty et al., 2012). The identification of effective treatments for metastatic disease suggests that these drugs may be applied even more successfully in patients in earlier stages of disease, such as stage II or III, where microscopic distant metastases may be eradicated by targeted therapies (Balch et al., 2009). However, identifying high-risk patients who should receive such postoperative "adjuvant" therapy is challenging using the current clinical staging, and would benefit from more reliable indicators of tumor invasiveness and recurrence risk. For patients with advanced melanoma, as well as those with localized disease, analysis of circulating tumor cells (CTCs) may therefore provide a novel biomarker to guide therapeutic decisions.

In addition to diagnostic applications, the detailed molecular characterization of melanoma cells circulating in the bloodstream may yield new insights into the process of melanoma metastasis (Liu et al., 2011; Ramsköld et al., 2012). However, there are significant challenges. CTCs are rare even in patients with advanced cancer. Moreover, melanomas do not express the classical epithelial cell surface marker EpCAM, which has formed the basis for most CTC isolation strategies (Yu et al., 2011). Some melanoma-specific cell surface epitopes have been proposed for CTC enrichment (Khoja et al., 2013), and the large size of tumor cells within primary melanomas has led to the application of filtering strategies to isolate melanoma CTCs (De Giorgi et al., 2010), although recent studies have suggested that melanoma CTCs may span a wide range of cell sizes (Ozkumur et al., 2013). Given the difficulty of isolating whole melanoma CTCs, RT-PCR-based measurements of blood-derived, melanoma-specific transcripts have also been employed. In patients with locally invasive tumors, positive PCR signals in such assays are associated with a poor prognosis and an increased risk of distant metastasis (Hoshimoto et al., 2012). Taken together, multiple approaches suggest the presence of melanoma cells in the bloodstream of patients in various stages of disease, but a robust cell-capture platform is essential for efficient detection and molecular characterization of these cells.

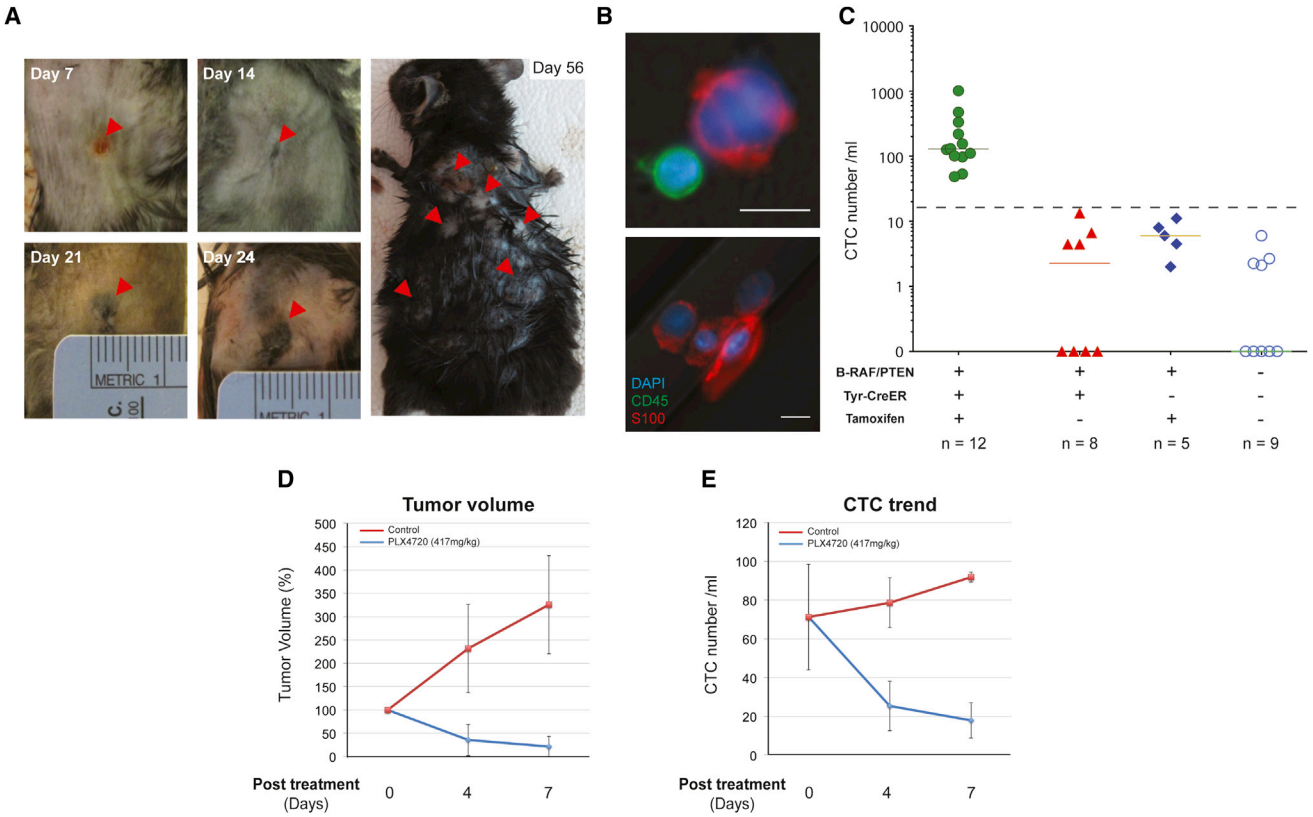

Figure 1. Identification of CTCs in the *B-raf*$^{CA/+}$/*Pten*$^{flox/flox}$ Mouse Melanoma Model

(A) Representative images of melanoma induced by focal tamoxifen injection. Arrowheads show tumor progression at the injection site from day 7 to day 24 (left) and cutaneous metastasis at day 56 after tumor induction (right).

(B) Upper: representative image of a mouse melanoma CTC adjacent to a leukocyte. Lower: a cluster of four CTCs. Blue, DAPI; green, CD45; red, S100. Scale bars, 10 μm.

(C) Quantification of CTCs from a cohort of tumor-bearing mice (green, n = 12) and control mice (red, genotype-matched tumor-free mice, n = 8; blue, Tyr-CreER− mice that received tamoxifen injection, n = 5; open circles, syngeneic C57BL/6 mice, n = 9). Solid lines, median CTC counts; dashed line, threshold of ≥14 S100$^+$ cells/ ml.

(D and E) Concordant changes in (D) tumor volume and (E) CTCs in tumor-bearing mice fed with control chow or PLX4720-containing chow (blue, PLX4720; red, control). Mean value, error bars represent SD.

See also Figure S1.

Here, we adapted a microfluidic platform, the ^{HB}CTC-Chip (Stott et al., 2010), to capture melanoma CTCs using panels of antibodies against melanoma-specific cell surface markers, followed by immunofluorescence (IF) staining for melanoma antigens and optimized on-chip imaging. We applied this ^{HB}CTC-Chip to a robust, inducible B-RAF-PTEN-driven mouse melanoma model (Dankort et al., 2009), in which we validated capture of bona fide melanoma CTCs and monitored their response to targeted therapy and the timing of CTC generation by localized lesions. The large number of CTCs generated in the mouse melanoma model, together with the consistent genetic background, allowed us to compare RNA sequencing (RNA-seq) profiles of matched primary tumors, metastatic lesions, and CTCs, thereby generating a melanoma CTC signature that identified high-risk subsets in human melanoma-derived specimens. Based on its validation in the mouse model, we applied the melanoma ^{HB}CTC-Chip to a pilot cohort of human samples.

RESULTS

Microfluidic Isolation of CTCs and Their Response to B-RAF-Targeted Therapy in a Mouse Melanoma Model

Given the considerable heterogeneity of human melanoma, we sought to adapt the ^{HB}CTC-Chip to capture cells from a genetically engineered mouse model of melanoma (Dankort et al., 2009). In this model, subcutaneous injection of tamoxifen at the flank of the animal leads to activation of oncogenic B-RAF^{V600E} coincidently with deletion of PTEN within melanocytes. Melanomas are formed at the injection site with 100% penetrance within 3 weeks, with distant cutaneous metastases appearing at 6–7 weeks (Figure 1A). After testing B-RAF/PTEN-driven mouse tumors for expression of multiple lineage-specific markers, we selected antibodies against the cell surface epitopes CSPG4 and MCAM for CTC capture, and antibody against the melanoma marker S100 for staining and imaging of captured CTCs (Figures S1A–S1D). We collected blood specimens from

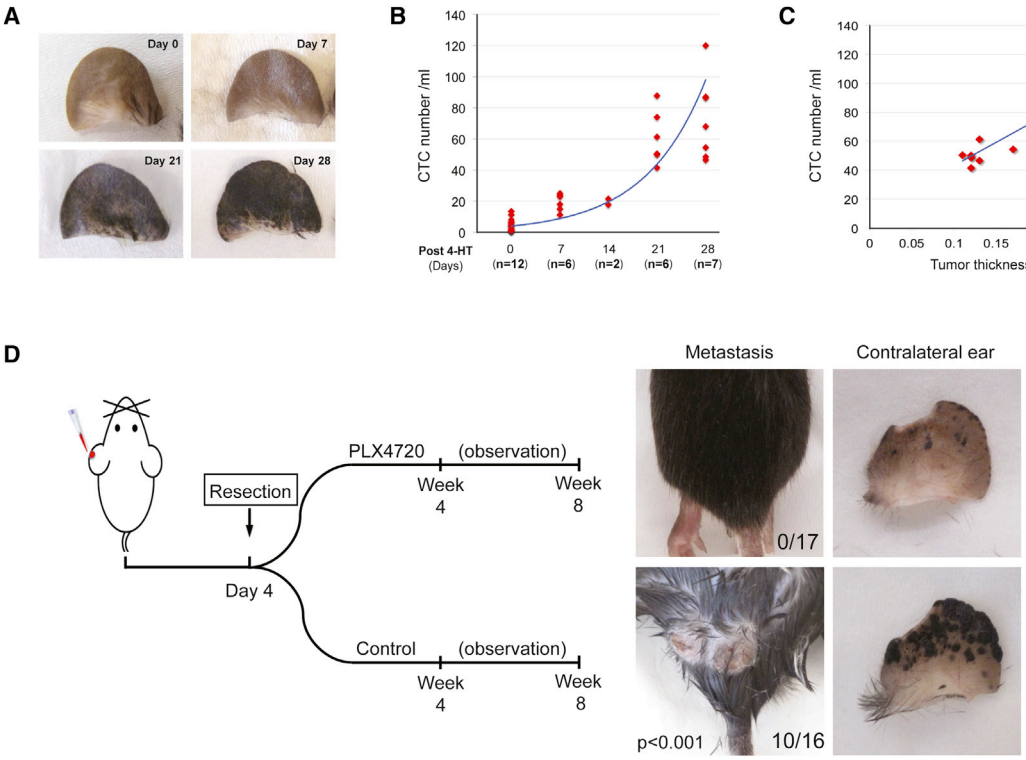

Figure 2. Distant Metastasis Is Associated with the Presence of CTCs and Is Prevented by Adjuvant B-RAF Inhibition

(A) Tumor progression on 4-HT-treated ears.

(B) CTCs can be detected as early as day 7 after tumor induction and correspond to tumor progression.

(C) CTC counts correlate with tumor thickness when thickness is >0.1 mm (n = 12, R^2 = 0.66).

(D) Left: schematic diagram of the experimental procedures. Right: postsurgical administration of B-RAF inhibitor delays or prevents distant metastasis. After the affected ears were removed, the mice were fed with PLX4720-containing chow (n = 17) or control chow (n = 16) for 4 weeks. Subcutaneous metastases were observed in the control group (10 out of 16), but not in the PLX4720-fed group (0 out of 17). Tumors on the contralateral ear were also largely suppressed by PLX4720.

See also Figure S2 and Table S1.

tumor-bearing mice (Yu et al., 2012) and processed the blood by passing it through anti-CSPG4 and anti-MCAM functionalized ^{HB}CTC-Chips.

Captured cells were stained for S100, and the common leukocyte markers CD45 and CTCs were defined as $S100^+/CD45^-$ (Figure 1B). As is done for all fluorescence-based CTC imaging, we set a baseline for positive scoring using tumor-free controls (Yu et al., 2012). Under the established imaging conditions, a median of two $S100^+/CD45^-$ cells/ml of blood (mean 3, range 0–13 cells/ml) was observed in nontumor-bearing mice (Tyr-CreER+ mice without tamoxifen treatment, n = 8; Tyr-CreER− mice with tamoxifen injection, n = 5; syngeneic C57BL/6 mice, n = 9). All of 12 melanoma-bearing mice (100%) scored positive for CTCs using a threshold of $\geq$14 $S100^+/CD45^-$ cells/ml, with a median of 114 cells/ml (mean 232, range 48–1,015 cells/ml) (Figure 1C). The CTCs were significantly larger than leukocytes (median size 14 μm, range 13–18 μm), and CTC clusters of two to four cells were also recovered (Figure 1B) as reported in other cancer types (Stott et al., 2010).

The CTC count rose progressively with increasing tumor burden following tumor induction (Figure S1E). Oral administration of the selective B-RAF inhibitor PLX4720 resulted in a concordant reduction in both the size of the primary tumor and the number of CTCs. A >50% drop in CTC numbers was evident as early as 4 days after initiation of PLX4720 therapy, and these numbers continued to decline progressively over the 14-day treatment period (Figures 1D, 1E, and S1F–S1H).

Prevention of Metastases from Early Melanomas by Postresection Administration of B-RAF Inhibitor

The efficient generation and capture of CTCs in a mouse melanoma model, coupled with our ability to monitor the earliest stages of tumor formation in the skin, made it possible to test the timeline of CTC generation and seek histopathological correlates within the primary tumor. For these experiments, we chose to apply minute amounts of the active tamoxifen metabolite 4-hydroxytamoxifen (4-HT) topically to the outer ear, thus avoiding skin trauma associated with subcutaneous injection and generating a small initial lesion amenable to detailed histopathological analysis. A darkening of the outer ear consistent with melanocyte proliferation was grossly evident 17–21 days after topical application of 4-HT (Figure 2A), and increasing CTC numbers were detectable in the circulation as early as 7 days (Figure 2B). Histopathological features analyzed in the primary melanoma

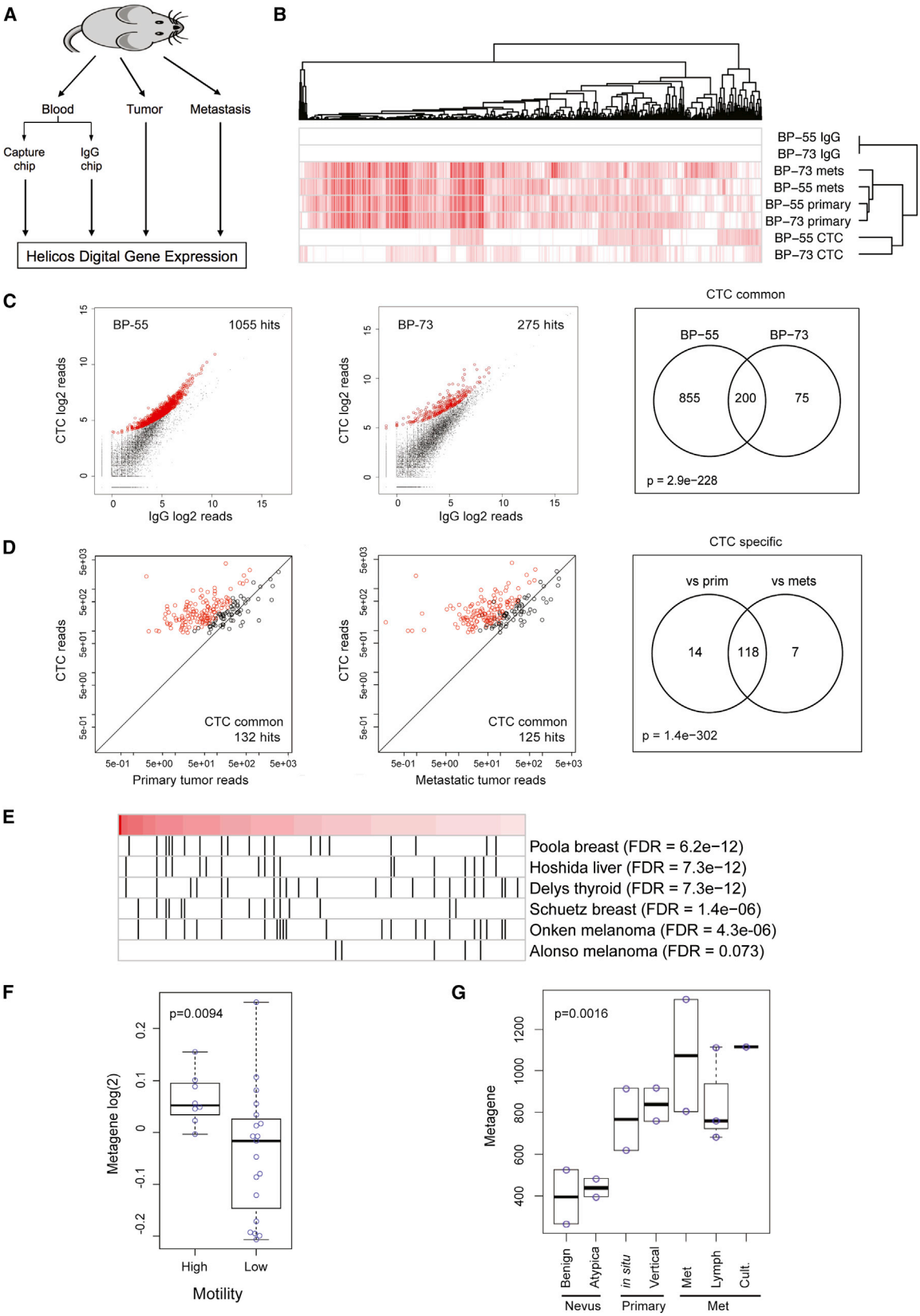

(legend on next page)

lesions included tumor thickness, tumor ulceration, tumor cell mitoses, and fat invasion (Table S1). Consistent with well-established predictors of clinical outcome (Carrillo et al., 2002), the thickness of the primary lesion was most highly correlated with increasing generation of CTCs (Figure 2C).

Initiation of melanoma in the mouse ear was followed by its appearance in the contralateral ear at 4 weeks and disseminated cutaneous spread (to the torso) at 7–8 weeks. We could not determine whether the early contralateral ear involvement represented true blood-borne metastasis with a predilection for the ear or, more likely, the effect of mouse grooming, which could spread the 4-HT by contact to the contralateral ear. Consistent with the rapid generation of CTCs in the mouse ear model, resection of the primary tumor as early as 4 days following 4-HT application did not prevent the subsequent development of distant metastases (Figures 2D and S2). As a potential model for the adjuvant treatment of early-stage melanoma, we tested whether resection of the primary tumor followed by a short course of B-RAF inhibition could delay or prevent the development of metastases. Of 16 mice treated with 4-HT followed by resection of the treated ear at day 4, ten (63%) developed distant cutaneous metastases at 2 months. Remarkably, none of 17 mice (0%) that received 4 weeks of postsurgical B-RAF inhibitor developed cutaneous metastases at 2 months ($p < 0.001$; Figure 2D). The appearance of tumors in the contralateral ear was significantly reduced, but not completely abrogated, by PLX4720 treatment. When compared with the time-limited efficacy of B-RAF inhibition in the setting of metastatic melanoma, these observations suggest that a brief treatment with B-RAF inhibitor in the postsurgical "adjuvant" setting, when tumor burden is low, may have a dramatic impact on the risk of tumor recurrence.

RNA-Seq Profile of Mouse Melanoma CTCs

The availability of matched primary melanoma, CTCs, and metastatic deposits in a genetically defined mouse model allowed us to compare expression profiles for these sequential stages of cancer dissemination. As previously described (Yu et al., 2012), we applied single-molecule, next-generation RNA-seq (Heliscope Single Molecule Sequencer) to avoid the loss of signal associated with PCR amplification of low-quantity, heterogeneous templates. The median purity of CTCs enriched by ^{HB}CTC-Chip from tumor-bearing mice was 0.3% (range 0.073%–3.85%, n = 12; Figure 1C), with higher purity achieved from mice with higher tumor burdens. We therefore selected another five mice with multiple metastatic lesions, obtained CTC-enriched populations, and subjected them to microfluidic in-line extraction of nucleic acids followed by RNA-seq. To allow digital subtraction of contaminating leukocyte transcripts from the CTC-enriched reads, each mouse-derived blood specimen was processed through paired ^{HB}CTC-Chips. One ^{HB}CTC-Chip was functionalized with antibodies to CSPG4 and MCAM (Capture-^{HB}CTC-Chip), and the other was mock functionalized with matching IgG (Control-IgG-Chip), which enabled us to achieve a more specific digital expression pattern for melanoma CTCs. We also processed primary and metastatic melanoma deposits using the same single-molecule sequencing platform (Figure 3A). Although expression differences between matched primary and metastatic tumors were evident, none of these differences were shared across the four pairs that were successfully sequenced (Figure S3). Therefore, we did not identify consistent metastasis-specific transcripts in this mouse model.

Of five mice analyzed, two (BP-55 and BP-73) had CTC-derived RNA of sufficient quality to generate data for detailed digital gene-expression profiling. Unsupervised clustering of the 1,000 genes with the highest SD suggested that the CTCs express a set of transcripts that are underrepresented in both primary and metastatic tumors (Figure 3B). Mice BP-55 and BP-73 respectively had 1,055 and 275 transcripts that were overexpressed (false discovery rate [FDR] $< 1 \times 10^{-05}$ and >2-fold) in CTC-enriched cells compared with mock-enriched controls, and 200 of these transcripts were shared between the two specimens (CTC-common; Figure 3C). Gene Ontology analysis applied to the 200 genes identified melanosome-associated genes (Table S2), reflecting the CTCs' melanocytic origin. Of these 200 CTC-common transcripts, 132 were specifically overexpressed in CTCs compared with the primary tumor reads (CTC-specific), 125 were overexpressed compared with metastatic tumor reads, and 118 were common to both gene sets (Figure 3D).

Figure 3. Digital Gene-Expression Analysis of Mouse CTCs

(A) Schematic diagram of the digital gene expression (DGE) experiment. RNA was extracted from Chip-enriched cells and matched primary and metastatic tumors, and subjected to Helicos DGE analysis.

(B) Unsupervised clustering of transcripts enriched in CTCs and primary and metastatic tumors from two mice (BP-55 and BP-73), demonstrating that the expression profiles of the CTCs are distinct from those of the primary and metastatic tumors.

(C) Genes upregulated in a CTC-enriched population compared with mock IgG-enriched cells. There were 1,055 (left) and 275 (middle) upregulated genes in samples BP-55 and BP-73, respectively, with an overlap of 200 genes (right, CTC-common).

(D) Of the 200 overlapping genes in (C), 132 were specifically overexpressed in CTCs compared with the primary tumor (left) and 125 were overexpressed in CTCs compared with the metastasis (middle); of these, 118 genes were common to both gene sets (right).

(E) GSEA on the 132 CTC-specific genes identified a number of gene sets related to cancer. Red bar, the 132 genes ranked by expression level from high (left, dark red) to low (right, light red); black vertical lines, overlap of the 132 genes with known gene sets. Poola breast, Poola invasive breast cancer genes (Poola et al., 2005); Hoshida liver, Hoshida liver carcinoma genes (Hoshida et al., 2009); Delys thyroid, Delys papillary thyroid cancer genes (Delys et al., 2007); Schuetz breast, Schuetz ductal invasive breast cancer genes (Schuetz et al., 2006); Onken melanoma, Onken aggressive uveal melanoma genes (Onken et al., 2006); Alonso melanoma, Alonso metastatic melanoma genes (Alonso et al., 2007).

(F) The signature of the 132 CTC-specific genes is associated with increased motility in melanoma cell lines (Jeffs et al., 2009).

(G) The signature also shows a progressive increase from benign or atypical nevus to primary and metastatic lesions. Benign, benign nevus; Atypica, atypical nevus; in situ, melanoma in situ; Vertical, melanoma vertical growth phase; Met, metastatic melanoma; Lymph, melanoma lymph node metastasis; Cult., metastatic melanoma short-term culture (Smith et al., 2005).

See also Figure S3 and Tables S2 and S3.

Gene set enrichment analysis (GSEA) applied to the 132 CTC-specific genes that were upregulated in CTCs versus primary tumors identified a signature that was previously implicated in noncanonical WNT, TGF-β, and BMP signaling (Hoshida et al., 2009; Figures 3E and S3C–S3F), as well as other gene sets implicated in tumor invasiveness in both melanomas and breast cancers (Onken et al., 2006; Poola et al., 2005; Schuetz et al., 2006). Also identified were gene sets driven by hyperactivation of the B-RAF^{V600E}-MAPK pathway in papillary thyroid cancer (Delys et al., 2007) and epithelial-to-mesenchymal transition (EMT) (Alonso et al., 2007) (Figure 3E).

We applied the mouse melanoma CTC-derived 132 metagene signature to expression data sets of human melanoma specimens, and the signature readily identified melanoma cell lines that were ranked as having a high cell motility score (Jeffs et al., 2009; Figure 3F). It also showed progressively increased expression in melanocytic lesions, ranging from benign or atypical nevi to primary and metastatic melanomas (Smith et al., 2005; Figure 3G). Thus, a set of transcripts that are upregulated during CTC generation in a mouse melanoma model may represent pathways that denote invasive properties in human melanoma.

Microfluidic Isolation of CTCs from Patients with Metastatic Melanoma

Our successful isolation of mouse melanoma CTCs raised the possibility that we could capture such cells from patient-derived blood specimens. Due to the highly heterogeneous expression of lineage markers in human melanomas (Herlyn and Koprowski, 1988), we screened 11 human melanoma cell lines for expression of 42 melanoma antigens (Figure S4). We selected a cocktail of 12 antibodies against melanoma cell surface epitopes that identified all 11 melanoma cell lines but reacted minimally to normal blood cells, demonstrating capture of >90% melanoma cells (Figure S4). A second cocktail of four distinct antibodies against melanoma epitopes was chosen to stain captured cells (melanoma stain [MEL], Figures 4A and S4; Table S4). As for the mouse CTCs, we set an imaging threshold using blood specimens from healthy donors. A median of 1 MEL^{+}/CD45^{-} cell/2.5 ml blood was observed in control specimens (range 0–2 cells/2.5 ml; n = 10), which led us to define ≥3 cells/2.5 ml as a positive CTC score. CTCs above this threshold were observed in 138 of 174 samples (79%) from 41 patients at various stages of treatment (median 8 cells/2.5 ml, range 0–132). Significantly higher numbers of CTCs ($p < 0.0001$) were identified from pretreatment samples (median 24 CTCs/2.5 ml, range 11–132; n = 21; Figure 4B). Captured melanoma CTCs exhibited a wide range of cell sizes (11–19 μm diameter) and CTC clusters (≥2 cells) were identified in three out of 174 samples (Figure S5F). Although the relatively low purity of human CTCs captured using this assay (median 0.07%, range 0%–0.77%) precluded the molecular analysis performed in the mouse model, it allowed us to monitor patients undergoing therapeutic interventions. In four patients with metastatic B-RAF^{V600E} melanoma who were receiving targeted anti-B-RAF therapies (two experiencing relatively durable responses [patients M1 and M2] and two having only transient benefit [patients M3 and M4]), CTC numbers were generally correlated with clinical evaluation of disease status (Figure 4C).

DISCUSSION

We have demonstrated the successful adaptation of a microfluidic device for melanoma CTC enrichment and applied it to a mouse model that recapitulates the biology of B-RAF-driven melanoma. The characterization of melanoma CTCs isolated in this model provides an initial insight into their invasive properties and sets the stage for potential future clinical applications. The mouse B-RAF/PTEN-driven melanoma model demonstrates a rise in CTC numbers as the primary tumor enlarges and metastases appear. Similarly, a brisk decline in CTCs concomitant with tumor shrinkage in response to targeted therapy is evident. Thus, in this genetically homogeneous model, CTC numbers are well correlated with tumor burden. In different human cancers, which exhibit considerable genetic heterogeneity, CTC numbers are notoriously variable across different individuals and are poorly correlated with radiographic measurements of tumor burden (reviewed in Yu et al., 2011). However, longitudinal follow-up of individual patients does show a correlation with tumor response or progression. Such a trend is also evident in the melanoma patients studied here, and it suggests that once the detection platforms for human melanoma CTCs are optimized, monitoring the number of these cells during therapy may help guide treatment for metastatic cancer.

Although most applications of CTC technologies have focused on monitoring advanced cancers, the highly invasive nature of cancer cells in this melanoma model made it possible to study their generation in the setting of early, localized disease. Indeed, in the mouse ear melanoma initiation model, we find that CTCs are shed very early into the circulation, at a time when the primary lesion is defined by an increase in pigmentation preceding the appearance of a tumor. Resection of the ear at this early stage does not prevent the development of distant cutaneous metastases, confirming the rapid blood-borne dissemination of tumor cells. Remarkably, a relatively brief course of B-RAF inhibitor therapy is sufficient to suppress the development of distant cutaneous metastases. Conceptually, these experiments lend support to the use of anti-B-RAF therapies in the postoperative adjuvant setting, where the relatively low tumor burden may allow the drug to kill all residual disease and prevent recurrence at distant sites. Two ongoing clinical trials (NCT01682083 and NCT01667419) are currently testing this hypothesis. However, identifying the subset of patients with stage II and III disease who are at high risk of tumor recurrence following resection of the primary lesion remains a major challenge, with histological hallmarks such as tumor thickness, ulceration, and mitotic rate enabling only incomplete patient stratification. Such patient stratification is essential given B-RAF inhibitor-related toxicity (Su et al., 2012). Optimization of human melanoma CTC-capture platforms may allow detection of rare cells in patients with early disease, potentially providing a predictive measure of recurrence risk. In this context, it is of interest that the ability of primary melanoma explants to generate CTCs following implantation into immunodeficient mice appears to be predictive of their recurrence risk (Quintana et al., 2012).

The gene-expression patterns correlated with melanoma aggressiveness have not been well defined, possibly reflecting the considerable heterogeneity in this disease (Schramm et al.,

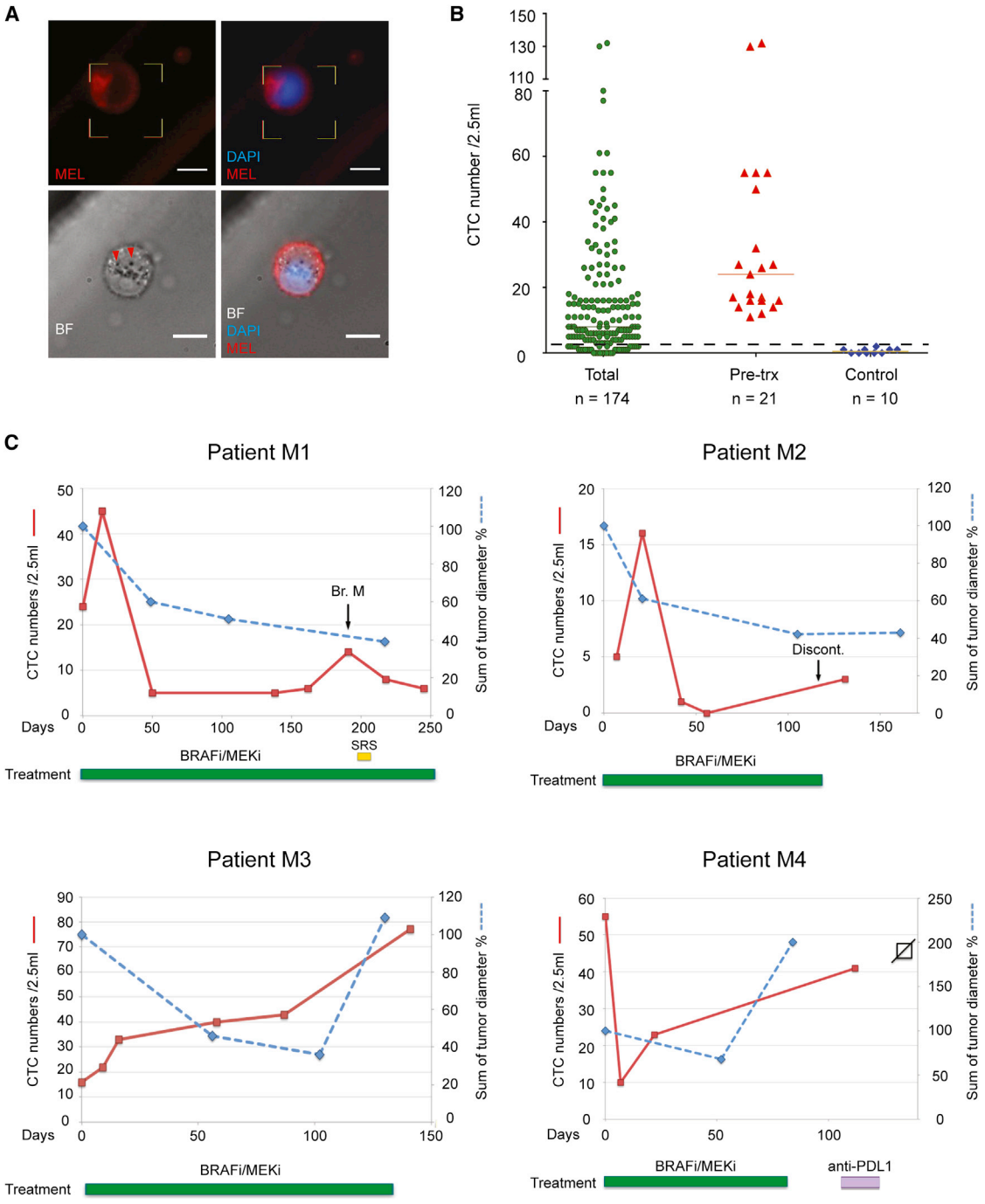

Figure 4. Detection and Characterization of CTCs in Melanoma Patients

(A) Representative images of CTCs from patients with metastatic melanoma. CTCs are defined as being MEL$^+$ and CD45$^-$. Upper: IF image of a MEL$^+$CD45$^-$ melanoma CTC. Lower: bright-field (BF) image and merged image IF and BF of a CTC reveals intracellular "granules" marked with arrowheads. MEL, CSPG4/MCAM/TYRP-1/αSMA antibody cocktail (upper) or CSPG4 (lower). Blue, DAPI; red, MEL. Scale bar, 10 μm.

(B) CTC counts of 174 samples from metastatic patients, 21 pretreatment samples, and 10 healthy donors. Median MEL(C/M/T/S)$^+$/CD45$^-$ cell count is 8 cells/2.5 ml for all patient samples, 24 cells/2.5 ml for pretreatment samples, and 1 cell/2.5 ml for controls. Solid lines, median CTC counts; dashed line, threshold of ≥3 cells/2.5 ml.

(C) CTCs display dynamic changes in patients and correlate with therapy responses. Blue curve, radiographic tumor measurement; red curve, CTC counts. Br. M, brain metastasis; SRS, stereotactic radiosurgery; Discont., treatment discontinued; B-RAFi/MEKi, dabrafenib/trametinib (patients M1, M3, and M4) or LGX818/MEK163 (patient M2).

See also Figure S4 and Table S4.

2012). In contrast, in the syngeneic mouse model, we were able to identify a small set of markers that were consistently upregulated in CTCs compared with either primary or metastatic tumors. Although the initiating B-RAF mutation triggered the melanoma model, CTCs demonstrated a further upregulation of B-RAF-MAPK activity (Figure 3E, Delys thyroid). Consistent with a B-RAF-MAPK-induced melanoma "dedifferentiation" phenotype (Frederick et al., 2013), expression of many melanocytic differentiation genes, including MITF, GP100, and Melan-A, was considerably lower in CTCs than in primary tumors (Figure S3G; X.L. and D.A.H., unpublished data). Even the "melanosome" genes expressed by CTCs were mainly genes whose products involve the maintenance of melanosome structures (e.g., ANXA2 and LAMP1), rather than the classic melanocytic differentiation genes (Table S2). The existence of melanoma stem cells remains controversial (Quintana et al., 2008), and we did not find any candidate melanoma stem cell-specific genes, including ABCB5 (Schatton et al., 2008), CD34, and CD271 (Boiko et al., 2010; Held et al., 2010), to be enriched in CTCs. Interestingly, we did note significantly increased expression levels of two master transcription factors involving in stem cell reprogramming, Klf4 and Myc, in the melanoma CTC populations (Table S3).

Canonical Wnt signaling has been shown to contribute to metastatic dissemination in the B-RAF/PTEN mouse model (Damsky et al., 2011), but the most striking component of the CTC signature identified here was a similarity to a liver carcinoma gene set linked to noncanonical Wnt, TGF-β, and BMP signaling pathways (Figure 3E, Hoshida liver; Figures S3C–S3F; Hoshida et al., 2009). That signature also emerged in CTCs derived from a mouse model of pancreatic cancer, where it was correlated with anchorage independent survival signals (Yu et al., 2012). This raises the intriguing possibility that a set of conserved CTC-specific gene-expression patterns may exist across different cancer types, linked to signaling pathways that regulate cell survival by normally adherent cells that travel in the bloodstream. Together, our results indicate that the mouse melanoma CTC signature we identified here is correlated with cellular invasiveness in human melanoma. If this is confirmed in larger clinical trials, such a CTC-derived expression signature may identify an aggressive subset of melanoma with a high risk of blood-borne metastatic spread and help guide the rational treatment of early disease.

Although ^{HB}CTC-Chip has been shown to be effective for capturing melanoma CTCs in the B-RAF/PTEN model, robust platforms for studying human melanoma CTCs have proved elusive, possibly due to the heterogeneity and phenotypic plasticity of human melanomas (Hoek et al., 2008). We found that we needed to use a larger number of antibodies to reliably capture human melanoma CTCs compared with mouse CTCs, which resulted in increased nonspecific binding by contaminating leukocytes and the need to perform complex chip functionalization protocols. As such, detailed molecular analysis of human melanoma CTCs will require single-cell isolation protocols, as well as nontumor epitope-driven CTC isolation platforms (Ozkumur et al., 2013; see Supplemental Discussion). Nonetheless, the human melanoma-specific ^{HB}CTC-Chip designed here allowed enumeration of CTCs from patients with metastatic disease, with a dynamic range that enabled longitudinal monitoring of treatment response and disease progression. Indeed, within the parameters of periodic sampling that was not timed to specific treatment evaluations or therapeutic interventions, we observed a general concordance between CTC numbers and clinical status in patients undergoing B-RAF-targeted therapies for metastatic melanoma. An unexpected finding in both human and mouse melanoma CTCs was the presence of CTC clusters (Figures 1B and S4F). Such groupings of CTCs in the circulation have been observed in patients with various epithelial cancers (Cho et al., 2012; Stott et al., 2010) and are likely a result of tumor fragments breaking off into the circulation. Primary melanocytes exist as single cells. As such, melanoma cells have not been thought to form strong intercellular adhesions; however, it was previously reported that artificially generated melanoma microemboli display increased tumorigenic potential compared with single melanoma cells (Fidler, 1973). Therefore, the origin and functional significance of melanoma CTC clusters, and their contribution to human melanoma metastasis, remain to be defined.

In summary, the analysis of melanoma CTCs in a well-defined and homogeneous mouse model, together with emerging data on human melanoma CTCs, is likely to provide important insights into the biological drivers of blood-borne invasion in this disease. The detection of CTCs in early invasive disease, as well as in established metastatic cancer, may help guide the application of increasingly powerful therapeutic regimens.

EXPERIMENTAL PROCEDURES

Detailed procedures and reagent information are provided in Supplemental Experimental Procedures.

ACCESSION NUMBERS

The RNA-seq data reported in this paper have been deposited in the GEO database under accession number GSE52031.

SUPPLEMENTAL INFORMATION

Supplemental Information includes Supplemental Discussion, Supplemental Experimental Procedures, four figures, and four tables and can be found with this article online at http://dx.doi.org/10.1016/j.celrep.2014.03.039.

ACKNOWLEDGMENTS

The authors thank C. Hart, A. McGovern, C. Koris, and the Massachusetts General Hospital clinical research coordinators for help with clinical studies; L. Libby for mouse studies; F. Ozsolak and P. Milos (Helicos) for RNA-seq; and J. Walsh, J. Lennerz, and M. Ulman for microscopy expertise. This work was supported by grants from Stand Up To Cancer (D.A.H., M.T., and S.M.), the Howard Hughes Medical Institute (D.A.H.), the Melanoma Research Foundation (X.L.), the National Foundation for Cancer Research (D.A.H.), and the NIH (NIH CA129933 to D.A.H. and NIBIB EB008047 to D.A.H. and M.T.). Massachusetts General Hospital has filed for patent protection for CTC technology.

Received: October 28, 2013
Revised: January 18, 2014
Accepted: March 12, 2014
Published: April 17, 2014

REFERENCES

Alonso, S.R., Tracey, L., Ortiz, P., Pérez-Gómez, B., Palacios, J., Pollán, M., Linares, J., Serrano, S., Sáez-Castillo, A.I., Sánchez, L., et al. (2007). A

high-throughput study in melanoma identifies epithelial-mesenchymal transition as a major determinant of metastasis. Cancer Res. *67*, 3450–3460.

Balch, C.M., Gershenwald, J.E., Soong, S.J., Thompson, J.F., Atkins, M.B., Byrd, D.R., Buzaid, A.C., Cochran, A.J., Coit, D.G., Ding, S., et al. (2009). Final version of 2009 AJCC melanoma staging and classification. J. Clin. Oncol. *27*, 6199–6206.

Boiko, A.D., Razorenova, O.V., van de Rijn, M., Swetter, S.M., Johnson, D.L., Ly, D.P., Butler, P.D., Yang, G.P., Joshua, B., Kaplan, M.J., et al. (2010). Human melanoma-initiating cells express neural crest nerve growth factor receptor CD271. Nature *466*, 133–137.

Carrillo, E., Prados, J., Melguizo, C., Marchal, J.A., Vélez, C., Serrano, S., Boulaiz, H., Mérida, J.A., and Aránega, A. (2002). Reverse transcriptase-polymerase chain reaction detection of circulating tumor cells in patients with melanoma: correlation with clinical stage, tumor thickness and histological type. Pathol. Int. *52*, 294–299.

Cho, E.H., Wendel, M., Luttgen, M., Yoshioka, C., Marrinucci, D., Lazar, D., Schram, E., Nieva, J., Bazhenova, L., Morgan, A., et al. (2012). Characterization of circulating tumor cell aggregates identified in patients with epithelial tumors. Phys. Biol. *9*, 016001.

Damsky, W.E., Curley, D.P., Santhanakrishnan, M., Rosenbaum, L.E., Platt, J.T., Gould Rothberg, B.E., Taketo, M.M., Dankort, D., Rimm, D.L., McMahon, M., and Bosenberg, M. (2011). β-catenin signaling controls metastasis in Braf-activated Pten-deficient melanomas. Cancer Cell *20*, 741–754.

Dankort, D., Curley, D.P., Cartlidge, R.A., Nelson, B., Karnezis, A.N., Damsky, W.E., Jr., You, M.J., DePinho, R.A., McMahon, M., and Bosenberg, M. (2009). Braf(V600E) cooperates with Pten loss to induce metastatic melanoma. Nat. Genet. *41*, 544–552.

De Giorgi, V., Pinzani, P., Salvianti, F., Panelos, J., Paglierani, M., Janowska, A., Grazzini, M., Wechsler, J., Orlando, C., Santucci, M., et al. (2010). Application of a filtration- and isolation-by-size technique for the detection of circulating tumor cells in cutaneous melanoma. J. Invest. Dermatol. *130*, 2440–2447.

Delys, L., Detours, V., Franc, B., Thomas, G., Bogdanova, T., Tronko, M., Libert, F., Dumont, J.E., and Maenhaut, C. (2007). Gene expression and the biological phenotype of papillary thyroid carcinomas. Oncogene *26*, 7894–7903.

Fidler, I.J. (1973). The relationship of embolic homogeneity, number, size and viability to the incidence of experimental metastasis. Eur. J. Cancer *9*, 223–227.

Flaherty, K.T., Hodi, F.S., and Fisher, D.E. (2012). From genes to drugs: targeted strategies for melanoma. Nat. Rev. Cancer *12*, 349–361.

Frederick, D.T., Piris, A., Cogdill, A.P., Cooper, Z.A., Lezcano, C., Ferrone, C.R., Mitra, D., Boni, A., Newton, L.P., Liu, C., et al. (2013). BRAF inhibition is associated with enhanced melanoma antigen expression and a more favorable tumor microenvironment in patients with metastatic melanoma. Clin. Cancer Res. *19*, 1225–1231.

Held, M.A., Curley, D.P., Dankort, D., McMahon, M., Muthusamy, V., and Bosenberg, M.W. (2010). Characterization of melanoma cells capable of propagating tumors from a single cell. Cancer Res. *70*, 388–397.

Herlyn, M., and Koprowski, H. (1988). Melanoma antigens: immunological and biological characterization and clinical significance. Annu. Rev. Immunol. *6*, 283–308.

Hoek, K.S., Eichhoff, O.M., Schlegel, N.C., Döbbeling, U., Kobert, N., Schaerer, L., Hemmi, S., and Dummer, R. (2008). In vivo switching of human melanoma cells between proliferative and invasive states. Cancer Res. *68*, 650–656.

Hoshida, Y., Nijman, S.M., Kobayashi, M., Chan, J.A., Brunet, J.P., Chiang, D.Y., Villanueva, A., Newell, P., Ikeda, K., Hashimoto, M., et al. (2009). Integrative transcriptome analysis reveals common molecular subclasses of human hepatocellular carcinoma. Cancer Res. *69*, 7385–7392.

Hoshimoto, S., Shingai, T., Morton, D.L., Kuo, C., Faries, M.B., Chong, K., Elashoff, D., Wang, H.-J., Elashoff, R.M., and Hoon, D.S.B. (2012). Association between circulating tumor cells and prognosis in patients with stage III melanoma with sentinel lymph node metastasis in a phase III international multicenter trial. J. Clin. Oncol. *30*, 3819–3826.

Jeffs, A.R., Glover, A.C., Slobbe, L.J., Wang, L., He, S., Hazlett, J.A., Awasthi, A., Woolley, A.G., Marshall, E.S., Joseph, W.R., et al. (2009). A gene expression signature of invasive potential in metastatic melanoma cells. PLoS ONE *4*, e8461.

Khoja, L., Lorigan, P., Zhou, C., Lancashire, M., Booth, J., Cummings, J., Califano, R., Clack, G., Hughes, A., and Dive, C. (2013). Biomarker utility of circulating tumor cells in metastatic cutaneous melanoma. J. Invest. Dermatol. *133*, 1582–1590.

Liu, Z., Fusi, A., Klopocki, E., Schmittel, A., Tinhofer, I., Nonnenmacher, A., and Keilholz, U. (2011). Negative enrichment by immunomagnetic nanobeads for unbiased characterization of circulating tumor cells from peripheral blood of cancer patients. J. Transl. Med. *9*, 70.

Onken, M.D., Ehlers, J.P., Worley, L.A., Makita, J., Yokota, Y., and Harbour, J.W. (2006). Functional gene expression analysis uncovers phenotypic switch in aggressive uveal melanomas. Cancer Res. *66*, 4602–4609.

Ozkumur, E., Shah, A.M., Ciciliano, J.C., Emmink, B.L., Miyamoto, D.T., Brachtel, E., Yu, M., Chen, P.I., Morgan, B., Trautwein, J., et al. (2013). Inertial focusing for tumor antigen-dependent and -independent sorting of rare circulating tumor cells. Sci. Transl. Med. *5*, 179ra147.

Poola, I., DeWitty, R.L., Marshalleck, J.J., Bhatnagar, R., Abraham, J., and Leffall, L.D. (2005). Identification of MMP-1 as a putative breast cancer predictive marker by global gene expression analysis. Nat. Med. *11*, 481–483.

Quintana, E., Shackleton, M., Sabel, M.S., Fullen, D.R., Johnson, T.M., and Morrison, S.J. (2008). Efficient tumour formation by single human melanoma cells. Nature *456*, 593–598.

Quintana, E., Piskounova, E., Shackleton, M., Weinberg, D., Eskiocak, U., Fullen, D.R., Johnson, T.M., and Morrison, S.J. (2012). Human melanoma metastasis in NSG mice correlates with clinical outcome in patients. Sci. Transl. Med. *4*, 159ra149.

Ramsköld, D., Luo, S., Wang, Y.C., Li, R., Deng, Q., Faridani, O.R., Daniels, G.A., Khrebtukova, I., Loring, J.F., Laurent, L.C., et al. (2012). Full-length mRNA-Seq from single-cell levels of RNA and individual circulating tumor cells. Nat. Biotechnol. *30*, 777–782.

Schatton, T., Murphy, G.F., Frank, N.Y., Yamaura, K., Waaga-Gasser, A.M., Gasser, M., Zhan, Q., Jordan, S., Duncan, L.M., Weishaupt, C., et al. (2008). Identification of cells initiating human melanomas. Nature *451*, 345–349.

Schramm, S.J., Campain, A.E., Scolyer, R.A., Yang, Y.H., and Mann, G.J. (2012). Review and cross-validation of gene expression signatures and melanoma prognosis. J. Invest. Dermatol. *132*, 274–283.

Schuetz, C.S., Bonin, M., Clare, S.E., Nieselt, K., Sotlar, K., Walter, M., Fehm, T., Solomayer, E., Riess, O., Wallwiener, D., et al. (2006). Progression-specific genes identified by expression profiling of matched ductal carcinomas in situ and invasive breast tumors, combining laser capture microdissection and oligonucleotide microarray analysis. Cancer Res. *66*, 5278–5286.

Smith, A.P., Hoek, K., and Becker, D. (2005). Whole-genome expression profiling of the melanoma progression pathway reveals marked molecular differences between nevi/melanoma in situ and advanced-stage melanomas. Cancer Biol. Ther. *4*, 1018–1029.

Stott, S.L., Hsu, C.H., Tsukrov, D.I., Yu, M., Miyamoto, D.T., Waltman, B.A., Rothenberg, S.M., Shah, A.M., Smas, M.E., Korir, G.K., et al. (2010). Isolation of circulating tumor cells using a microvortex-generating herringbone-chip. Proc. Natl. Acad. Sci. USA *107*, 18392–18397.

Su, F., Viros, A., Milagre, C., Trunzer, K., Bollag, G., Spleiss, O., Reis-Filho, J.S., Kong, X., Koya, R.C., Flaherty, K.T., et al. (2012). RAS mutations in cutaneous squamous-cell carcinomas in patients treated with BRAF inhibitors. N. Engl. J. Med. *366*, 207–215.

Yu, M., Stott, S., Toner, M., Maheswaran, S., and Haber, D.A. (2011). Circulating tumor cells: approaches to isolation and characterization. J. Cell Biol. *192*, 373–382.

Yu, M., Ting, D.T., Stott, S.L., Wittner, B.S., Ozsolak, F., Paul, S., Ciciliano, J.C., Smas, M.E., Winokur, D., Gilman, A.J., et al. (2012). RNA sequencing of pancreatic circulating tumour cells implicates WNT signalling in metastasis. Nature *487*, 510–513.

SUPPLEMENTAL DISCUSSION

The Herringbone ^{HB}CTC-Chip used in this paper has been reported as a technology to enrich for CTCs from epithelial cancers (eg. breast, prostate and lung) (Stott et al., 2010) and the current studies extend its application to melanoma, which express different and more heterogeneous cell surface antigens than most epithelial cancers. While these proof of principle experiments provide insight into the biology of melanoma metastasis, the ^{HB}CTC-Chip platform is not sufficiently robust for routine clinical application in patients with metastatic melanoma. Ongoing work is aimed at developing a robust, clinical grade platform for tumor-epitope independent CTC capture (Ozkumur et al., 2013).

SUPPLEMENTAL EXPERIMENTAL PROCEDURES

Mouse tumor tissue and cell line. The mouse melanoma cell line was generated from the established B-RAF$^{V600E/+}$; PTEN$^{-/-}$ tumor following collagenase IV (Sigma) digestion. Cells suspended in PBS were deposited onto a microscopic slide by Cytospin (Thermo Scientific) and stained with antibodies against CSPG4 (R&D Systems, Clone LHM-2) and MCAM (Miltenyi Biotec, Clone LSEC). The immunofluorescent (IF) staining procedures for mouse melanoma FFPE sections are listed as the following. Briefly, paraffin-embedded mouse melanoma sections were deparaffinized followed by heat mediated antigen retrieval (50mM Tris-HCl pH9.0, 100 °C for 20 minutes). After blocking with 1%BSA-PBS, the slides were incubated with primary antibodies (rabbit anti-S100, DAKO, 1:400; mouse anti-GP100, clone HMB45, Santa Cruz, 1:200) in blocking solution (1%BSA and 0.1% Triton-X in PBS) overnight at 4°C. Secondary antibodies used were goat anti-mouse Alexa Fluor 488(Invitrogen, 1:500) and goat anti-rabbit Alexa Fluor 594 (Invitrogen, 1:500). Nuclei were counter-stained with Hoechst (1:20000 in PBS). Images were taken on a fluorescent microscope (Nikon Eclipse 90i).

Mouse tumor induction and *in vivo* PLX study. All the animal procedures were approved by the MGH Subcommittee on Research Animal Care (SRAC). The *B-raf*$^{CA/+}$*/Pten* $^{flox/flox}$*/Tyr-CreER* mouse was described previously (Dankort et al., 2009) and was backcrossed into C57BL/6 genetic background. For tumor induction, the mice received either 1) focal subcutaneous injection of regular tamoxifen (Sigma T5648) (50ul at 5mg/ml in 50% EtOH suspension) at the flank (Figure 1) at 6-7 weeks after birth or 2) topical application of the active

metabolite of tamoxifen, 4-hydroxytamoxifen, 4-HT, (1ul at 20mg/ml in 100% EtOH) (Sigma H7904) at the left ear (Figure 2) at 24-27 days after birth. For subcutaneous injection-induced tumors, the mice were sacrificed at day 7, 14, 21, 28, 35 or 56 for CTC analysis (Figure 1, S1). In mice with ear tumors, the mice were sacrificed at day 7, 14, 21 and 28 to enumerate their CTCs (Figure 2). Corresponding tumor specimens were collected at the necropsy and immediately fixed with 4% formaldehyde.

In the mouse ear tumor surgery model, the 4-HT treated ears were surgically removed at day 4, 7, 14, 21 or 28 after tumor induction. Buprenex was given at 0.1mg/kg for each mouse 30 minutes prior to the surgery followed by 2 more doses at 12 and 24 hours post-procedure. All ear samples were immediately fixed (4% formaldehyde) and paraffin embedded. Tumors were graded and surgical margins were determined free of tumor cells by a Board-certified pathologist (negative surgical margins not obtained from day 21 and 28 tumors due to tumor progression).

For *in vivo* PLX4720 study, animals were given mouse chow containing 417mg/kg (Figure 1, S1), 200mg/kg PLX4720 (Plexxikon) (Figure S1) or control chow. For mice that received tamoxifen injection, special diets were given at post-injection day 28 for 4, 7 (Figure 1) or 14 days (Figure S1) until sacrifice. For mice that received 4-HT ear application, special food was given post-operatively for 4 weeks.

Mouse blood processing, CTC staining and enumeration. ^{HB}CTC-Chips were manufactured as previously described (Stott et al., 2010). Mouse ^{HB}CTC-Chips were functionalized with biotinylated anti-CSPG4 (R&D, Clone LHM-2) and anti-MCAM (Miltenyi Biotec, Rat IgG, Clone LSEC) for CTC capture or isotype control biotinylated mouse IgG1 and Rat IgG (BioLegend).

For mouse blood processing, approximately 0.9-1ml of blood was collected from each mouse by cardiac puncture and immediately diluted 1:1 with PBS-10mM EDTA pH 7.4. About one milliliter of diluted blood was subsequently processed through the chip using a syringe pump (Harvard Apparatus) at 1.25ml/hr followed by PBS flush (Yu et al., 2012) followed by either 4% paraformaldehyde fixation or RNA extraction.

For IF staining of mouse ^{HB}CTC-chips, following the blood run, cells that remained on the chip were fixed with 4% paraformaldehyde, permeabilized with 1% NP-40 in PBS and blocked with 3%BSA/2% donkey serum in PBS. Primary antibodies for in-line staining of mouse ^{HB}CTC-chips were anti-CD45 (R&D Systems, goat, 1:500) and anti-S100 (DAKO, rabbit, 1:400). Secondary antibodies were donkey anti-goat Alexa Fluor 488 (Invitrogen, 1:500) and donkey anti-rabbit Alexa Fluor 594 (Invitrogen, 1:500). Nuclei were stained with DAPI (Invitrogen, 1:1000). The chips were automatically imaged using the BioView imaging system (BioView Ltd.) at 10x magnification followed by automated imaging at 40x (BioView) or 60x magnification (Nikon Eclipse 90i). Cells positive for CTC markers but not CD45 were scored as potential CTCs and were subsequently subject to manual review. Detection baselines were determined based on specimen from three types of tumor-free mice including a) genotype-matched un-induced mice (n = 8), b) mice carrying *B-raf* $^{CA/+}$/*Pten* $^{flox/flox}$ but lacking the critical *Tyr-CreER* that received subcutaneous injection of tamoxifen (n = 5) and c) syngeneic C57BL/6 mice (n = 9) (purchased from the Jackson Laboratory). CTC counts were presented as CTCs per milliliter of whole blood.

RNA extraction and single molecule sequencing. Eight weeks after tamoxifen injection, blood samples were collected from mice (n = 5) with very high tumor burden, split and processed through the ^{HB}CTC-chips functionalized with anti-CSPG4/MCAM antibody and control IgGs, respectively. Matched primary (from the tamoxifen injection site) and metastatic (from upper or lower back) tumors were harvested from the same mouse and immediately flash-frozen in liquid nitrogen.

RNA extraction and single molecular sequencing was described previously (Yu et al., 2012). Briefly, RNA from fresh frozen tumor tissues was extracted using RNeasy MiniElute kit (Qiagen). RNA from Chip-captured cells was extracted and purified using RNeasy MicroKit (Qiagen) followed by cDNA synthesis using SuperScript III kit (Invitrogen). cDNAs were then poly-A tailed at the 3' end and subject to single molecule sequencing (Helicos Biosciences).

Bioinformatics analysis. Digital Gene Expression (DGE) analysis is performed as previously described (Yu et al., 2012). For unsupervised clustering analysis, we excluded all genes with any reads in the mock (IgG) control ^{HB}CTC-Chip and all genes with no reads in the CTC, primary or metastasis. The log(reads) of the genes with the 1000 highest standard deviation were submitted to average linkage agglomerative hierarchical clustering with distance defined as 1 – correlation coefficient. The DGE profiles were compared as previously described (Yu et al., 2012) with threshold for statistical significance a Benjamini–Hochberg q-value of 10^{-5} and a fold-change threshold of 2. Hypergeometric gene set enrichment analysis (hGSEA) was done as previously described (Yu et al., 2012) using genes sets obtained from MSigDB v 3.0 (Broad Institute) with an FDR threshold of 10%. Metagene values were computed as the mean log2(expression) (Fig 3F) or expression (Fig 3G) for all the genes in the gene set. If multiple rows of the expression matrix mapped to the same gene, the row with the maximum standard deviation was used. P-values for trends in metagene values were computed by the Wilcoxon test (Fig. 3F) or the likelihood ratio test applied to the cumulative link model with logit link function as implemented in version 2012.09-11 of the R-project package "ordinal" (Fig 3G).

Human cell lines, flowcytometry and IF staining. Human melanoma cell lines were cultured in RPMI-1640 media with 10% fetal bovine serum (FBS) and 1% Pen/Strep. SK-MEL-28 and MeWo were purchased from ATCC. 501MEL, M14, MALME-3M, SK-MEL-2, SK-MEL-5, UACC62 were a gift from Dr. David E. Fisher. SK-MEL-3, HT-144 and WM266-4 were a gift from Dr. Cyril Benes.

Cultured melanoma cells were dissociated from plates using either Accutase (eBioscience) or enzyme-free cell dissociation buffer (GIBCO). Cells were re-suspended and blocked in 1%BSA/1%FBS-PBS for 20min and subsequently stained with either primary antibody or isotype control in blocking buffer for 30min at 4°C. Alexa Fluor 647-conjugated secondary antibodies were used to amplify the signal. After washing, each sample was re-suspended and post-fixed with 500ul of 1% paraformaldehyde before being analyzed on a cytometer (BD LSRII). For IF staining, cells were fixed (4% paraformaldehyde), permeabilized (1% NP-40-PBS) and blocked (3% BSA-PBS) prior to antibody incubation.

Patient ^{HB}CTC-Chip optimization and blood specimen processing. For human ^{HB}CTC-Chip optimization, efficiency of cell capture was determined using pre-labeled (Celltracker Orange, Invitrogen), defined numbers of cancer cells spiked into control blood and processed through ^{HB}CTC-Chip. Cancer cell capture efficiency was calculated based on the number of cells retained on the ^{HB}CTC-Chip versus the number of cells that ran through the chip.

^{HB}CTC-Chips for patient specimens were functionalized with biotinylated antibodies against 12 human melanoma antigens (Table S4). The most critical antibodies for successful melanoma CTC capture targeted CSPG4 (present on 8 out of 11 human melanoma cell lines), p97/melanotransferrin (8 out of 10) and MCAM (8 out of 11) epitopes (X.L. and D.H., unpublished data), which in combination allowed ^{HB}CTC-Chip capture of cultured SK-MEL-28 cell with >90% efficiency (Figure S4). The additional nine antibodies (Table S4) were derived from pairwise comparisons and optimization using clinical specimens, and together, their inclusion increased the number of patient melanoma CTCs captured by up to five-fold. In brief, anti-CSPG4 (mouse IgG1, Clone LHM-2), EphA2 (goat), c-Met (goat) and A2B5 (mouse IgM) were from R&D Systems. Anti-MCAM (mouse IgG1, Clone P1H12) and NGFR (mouse IgG1, Clone NGFR5) were purchased from Abcam. Anti-c-kit (mouse IgG1, Clone 104D2), CD90 (mouse IgG1, Clone 5E10) and HNK-1 (mouse IgM) were obtained from BioLegend. Anti-N-Cadherin (mouse IgG1, Clone 8C11) was from eBioscience. Cetuximab (ImClone), a chimeric antibody against human EGFR, was biotinylated in house. Anti- p97/melanotransferrin (mouse IgG1, Clone L235) was purified from the culture supernatant of a hybridoma cell line (ATCC, HB-8446) and biotinylated by Covance.

In-patients with metastatic melanoma were enrolled according to an institutional review board, IRB, approved protocol (05-300). Blood samples from healthy volunteers were collected under a separate IRB-approved protocol. All blood specimens were collected between 8am and 2pm. All blood samples from the same patient were collected within the same 2-hour window across multiple appointment dates.

All human blood specimens were processed as described previously (Stott et al., 2010). In brief, patient blood samples were collected into vacutainer tubes (BD) and processed through ^{HB}CTC-

Chip within 4 hours of blood draw. About 2.5ml of blood was driven through the chip using the microfluidic-processing machine described previously (Stott et al., 2010) at a flow rate of 1.25ml/hr followed by a 2.5ml of PBS flush at 2.5ml/hr. 4% paraformaldehyde was subsequently delivered to the ^{HB}CTC-chips to fix the retained cells.

Patient CTC staining and enumeration. Primary antibodies for human ^{HB}CTC-chips IF staining were anti-CSPG4 (Abcam, mouse IgG2a, Clone 9.2.27, 1:100), anti-MCAM (BioLegend, mouse IgG2a, Clone SHM-57, 1:200), anti-TYRP1 (Abcam, mouse IgG2a, Clone TA99, 1:200), anti-αSMA (Sigma, mouse IgG2a, Clone 1A4, 1:400) and anti-CD45 (Santa Cruz, Rat IgG, Clone 3H1363, 1:400). The antibodies against MCAM and CSPG4 used in CTC IF staining were distinct from those used as capture antibodies (Table S4). Secondary fluorescent-conjugated antibodies were goat anti-mouse IgG2a Alexa Fluor 594 (Invitrogen, 1:500) and goat anti-Rat Alexa Fluor 488 (Invitrogen, 1:500). Human ^{HB}CTC-Chips were imaged the same way as for mouse chips. Detection threshold was set based on specimens from healthy volunteers. In all cases, CTCs were scored blind without prior knowledge of clinical history.

Patient tumor assessment was performed using Response Evaluation Criteria in Solid Tumors (RECIST) from restaging imaging performed every 6-8 weeks.

SUPPLEMENTAL FIGURES

Figure S1: Characterization of the mouse melanoma CTC model. (A-D) Marker expression in mouse melanomas. (A and B) IF staining of tumor-derived cell line demonstrated the expression of CSPG4 (A) and MCAM (B). (C and D) IF staining of tumor sections revealed the expression S100 (C) and GP100 (D) in tumor cells (asterisk, epidermis; arrowheads, basal layer; arrow, tumor). (E) CTC numbers correlate with tumor progression. Number of CTCs increase significantly after tumor initiation. (F) Mouse melanoma responded to selective B-RAF inhibitor PLX4720 showing dramatic tumor shrinkage as early as 4 days after treatment initiation (see main text for tumor volume quantification). (G-H) Prolonged PLX4720 exposure reduces CTC counts in a dose-dependent manner. (G) Representative images of mice on control chow (top panel) or 417mg/kg PLX4720 chow (bottom panel) for 2 weeks. (H) CTCs responded to B-RAF inhibitor in a dose-dependent manner (blue squares, CTCs from mice on control diet; pink diamonds, CTCs from mice fed with 200mg/kg PLX4720; red triangles, CTCs from mice fed with 417mg/kg PLX4720).

Figure S2: Surgery alone does not lead to a cure of early melanoma in mice. Ear was resected at day 7, 14, 21 or 28 after 4-HT application. Mice were monitored for another 8 weeks after surgery for the appearance of metastatic tumors.

Figure S3: Transcriptome analysis in primary, metastatic tumors and CTCs (A) Genes upregulated in metastatic tumor compared with the matched primary tumor were intersected across different mice (n = 4, from mice BP-53, BP-55, BP-72 and BP-73). Minimal overlap of genes was found in this comparison. (B) Similarly, genes downregulated in metastatic lesions compared with the primary tumor also displayed minimal overlap across the same 4 samples. (C-F) Hoshida liver carcinoma gene set was significantly enriched in CTCs. Hoshida gene signature was found to be overrepresented not only in CTC-enriched genes (genes upregulated by >2-fold in Chip-enriched cells compared with mock-enriched cells, C and E) but also in CTC-specific genes (CTC-enriched genes specifically overexpressed by >2-fold compared to the primary tumor, D and F). (G) Expression of MITF is lower in CTCs. Compared to normal melanocytes and primary tumor cells, CTCs express lower level of MITF (n= 4, from mice BP-53, BP-55, BP-72 and BP-73; rpm, reads per million).

Figure S4: Optimization of melanoma ^{HB}CTC-Chip for patient. (A) A list of candidate antigens tested for human ^{HB}CTC-Chip. Top panel, melanoma cell surface markers intended for both CTC immunoaffinity isolation and subsequent immunofluorescence (IF)-based CTC identification. Bottom panel, cytoplasmic or nuclear antigens intended for IF-based CTC detection only. Bold, antigens chosen for CTC applications; asterisk, antigens used for both CTC capture and IF detection (note: regarding such antigens, distinct antibodies were used). (B) IF staining of melanoma cell lines, SK-MEL-28 and UACC62, using CTC detection antibody cocktail (red, detection antibody staining; blue, DAPI nuclear staining). Differential expression of melanoma antigens was evident in the two cell lines. (C-E). Combinatorial uses of capture antibodies improved CTC capture efficiency. (C) SK-MEL-28 expresses CSPG4 (blue peak), p97 (green peak) and MCAM (orange peak) at different levels as determined by flowcytometry. (D) More than 90% of SK-MEL-28 cells were recovered on ^{HB}CTC-Chip with an antibody cocktail against CSPG4/MCAM/P97 compared to CSPG4/MCAM or CSPG4 alone (total amount of antibody on each ^{HB}CTC-Chip was 10ug equally split between different antibodies). (E) Increased CTC yield (>2-fold) from patient blood (M5) was observed when MCAM was incorporated into the capture antibody cocktail (total antibody on each chip was 10ug; CSPG4/MCAM/P97-1 and CSPG4/MCAM/P97-2 represent two ^{HB}CTC-Chips serving as technical replicates). (F) Representative images of a patient CTC cluster (M6). DAPI, blue; MEL, red; scale bar, 10μm.

Figure S1: Characterization of mouse melanoma and CTCs. (Related to Figure 1)

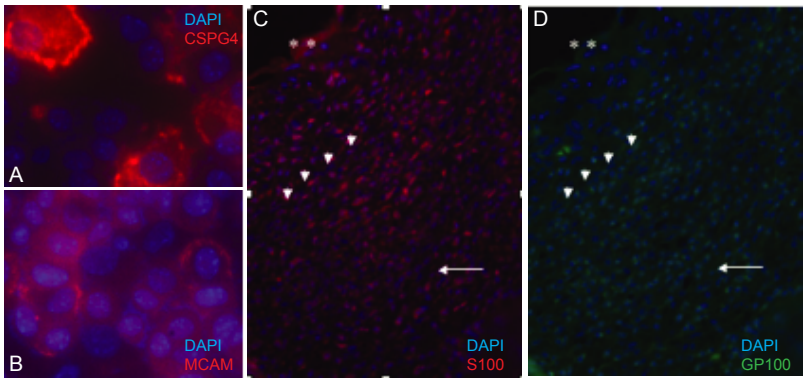

E

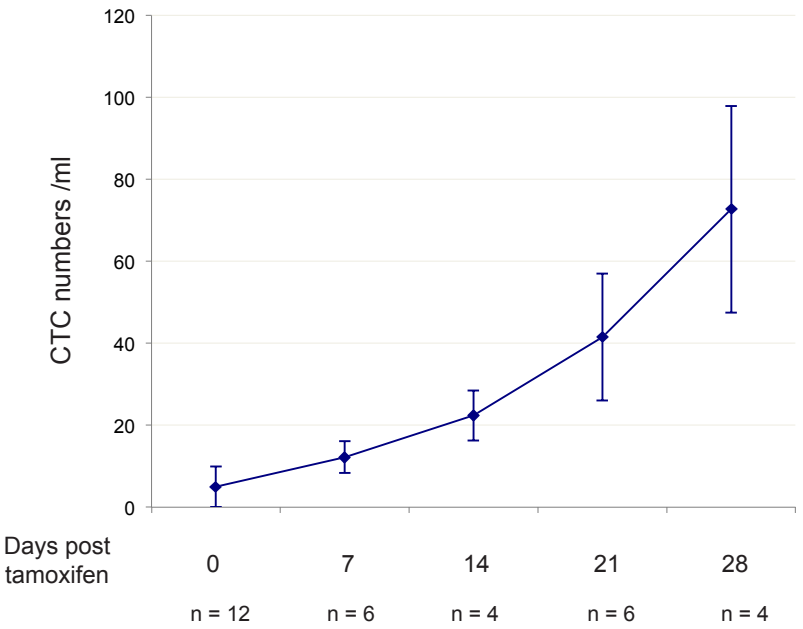

F

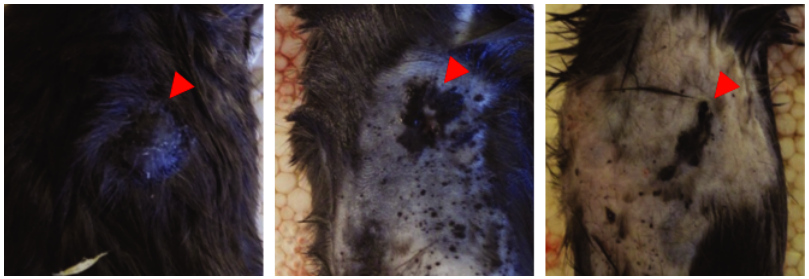

G

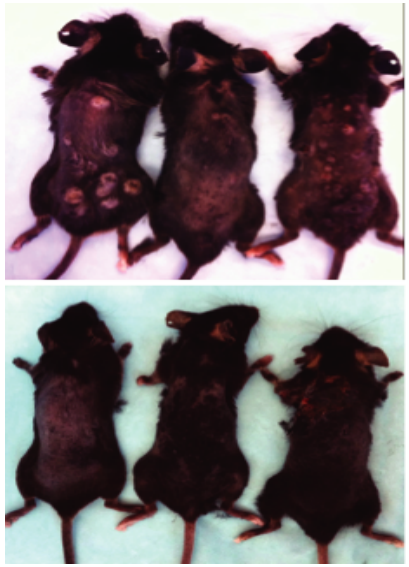

H

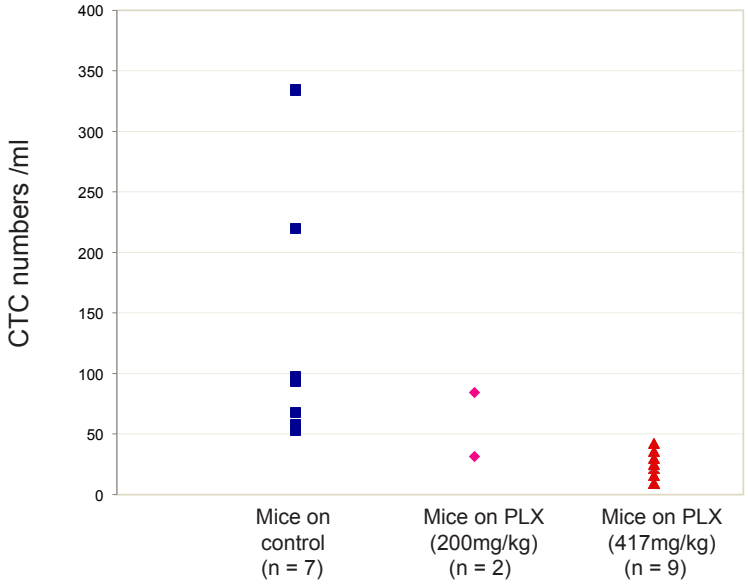

Figure S2: Mouse melanoma surgery model. (Related to Figure 2)

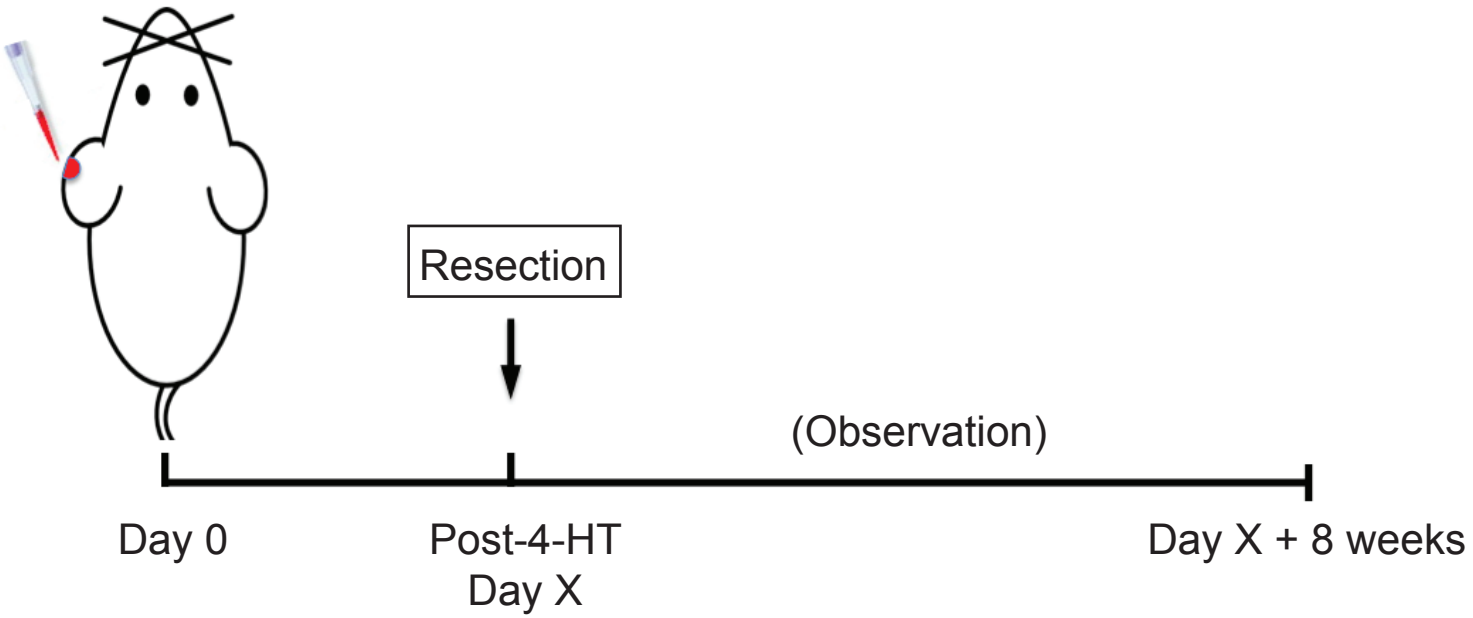

Resection post 4-HT (days)	Mice with met. tumor/total mice
7	11/11
14	7/7
21	5/5
28	3/3

Figure S3: Data analyses of the RNA-Sequencing experiment. (Related to Figure 3)

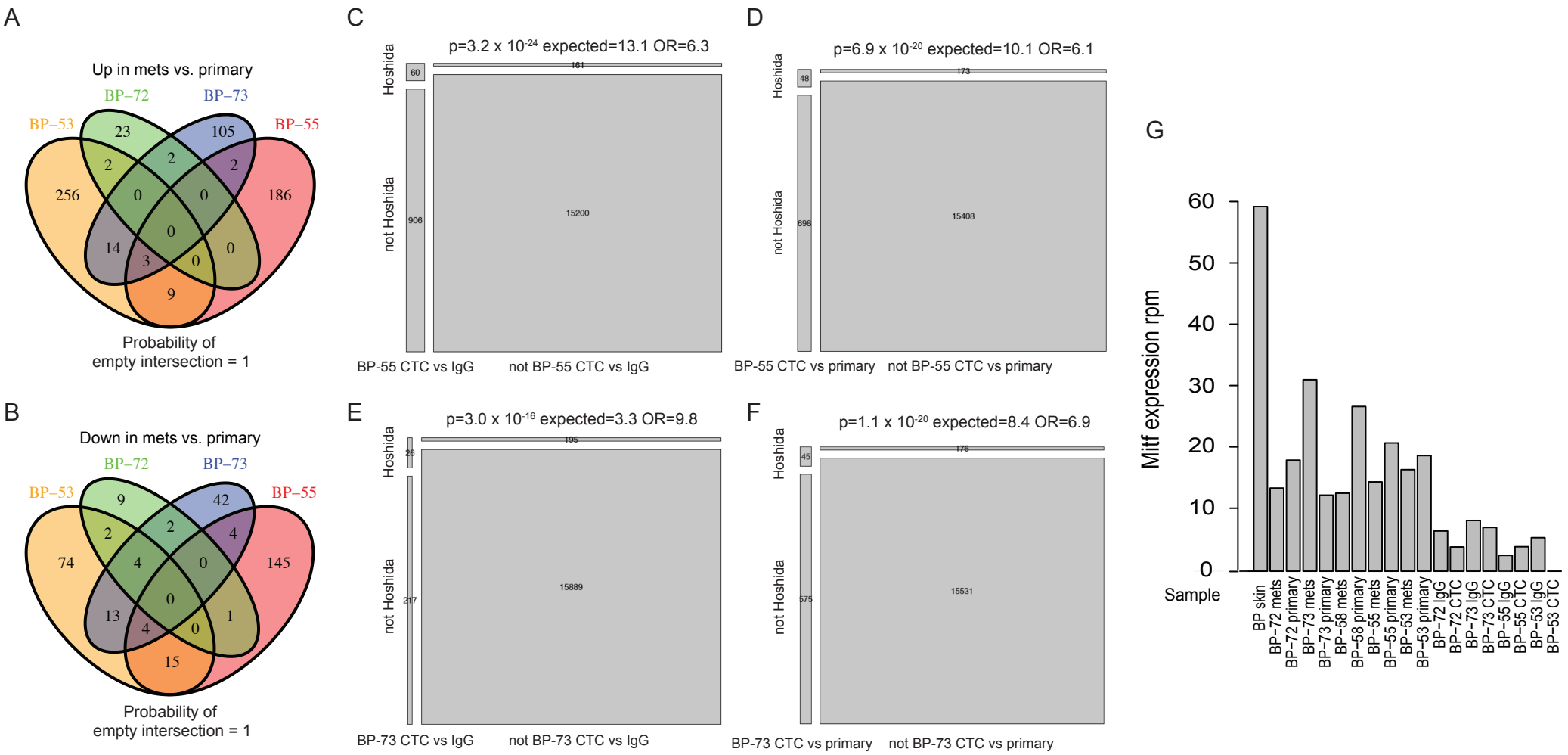

Figure S4: The construction and optimization of ^{HB}CTC-Chip for patient CTC enrichment. (Related to Figure 4)

A

Cell Surface Markers					
A2B5	**CD90**	**CD117**	**c-Met**	**CSPG4***	**EGFR**
EPHA2	**HNK-1**	**MCAM***	**NCad**	**NGFR**	**P97**
CD63	CDH19	ERBB2	ERBB3	GD2	GD3
KCad	O1	O4			

Cytoplamsic/nuclear markers					
aSMA	**TYRP-1**	GalNAc-T	GP100	MageA	MAP2
MelanA	MITF	NESTIN	Pax3	PIAS3	PRAME
S100	SOX2	SOX9	SOX10	SLUG	SNAIL
TYRP-2	TUJ1	TYR			

B

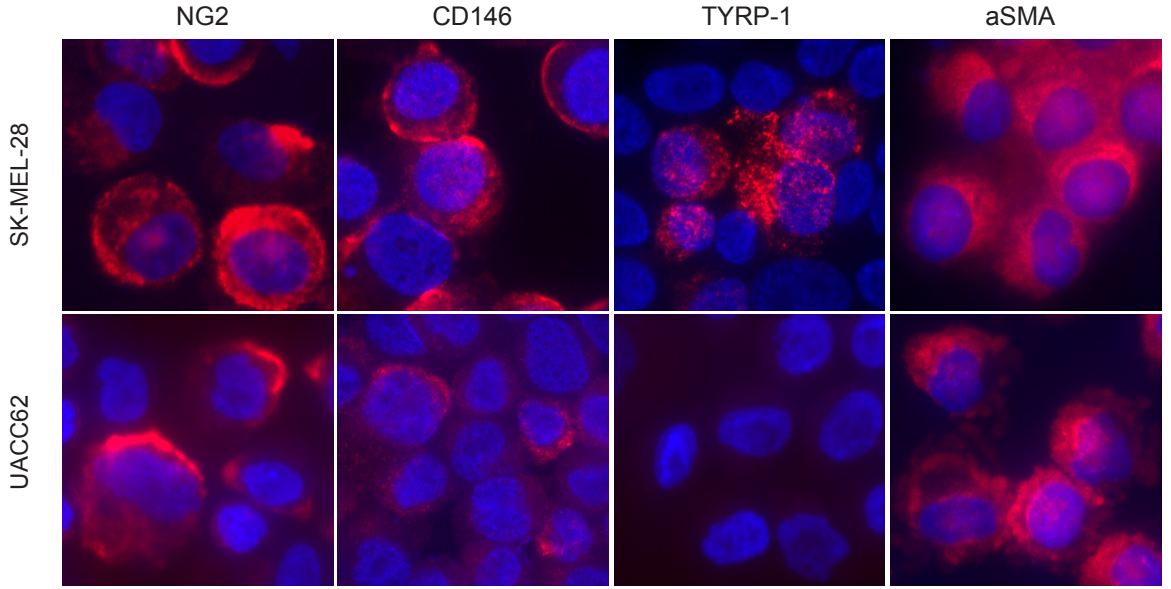

C

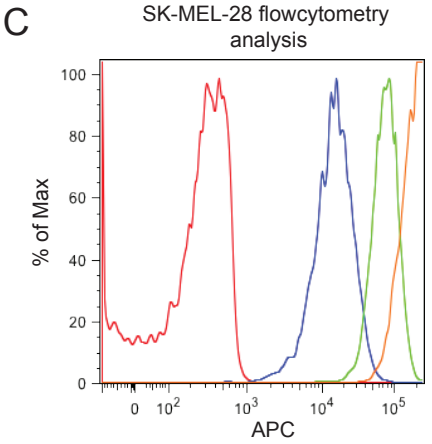

D

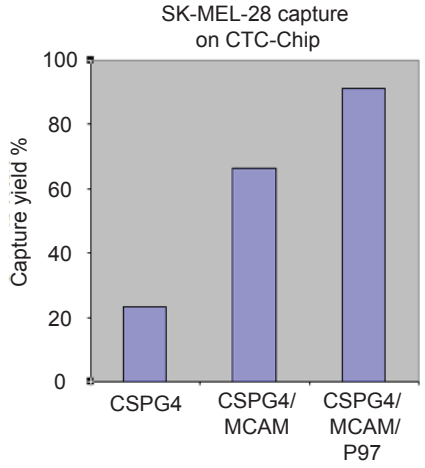

E

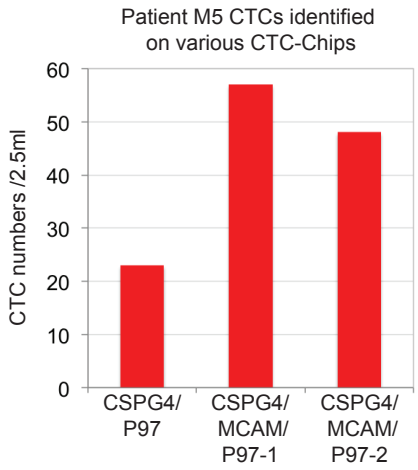

F

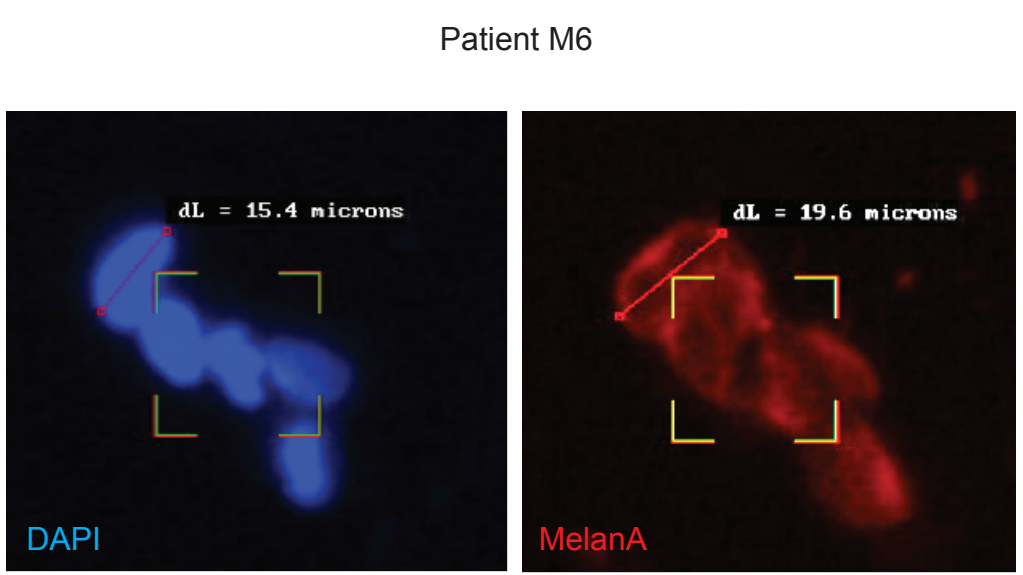

Table S1: Histological analysis of early mouse tumors. (Related Figure 2)

Mouse ID	BP154	BP156	BP157	BP160	BP161	BP162	BP163	BP164	BP167	BP168	BP177	BP178
CTC counts /ml	73.8889	50.0588	61.2222	68	48.5556	46.4444	86.5556	120	41.4	50.4	54.4	86.95
Tumor thickness (mm)	0.2	0.12	0.13	0.27	0.12	0.13	0.2	0.27	0.12	0.11	0.17	0.2
Ulceration	absent	absent	absent	absent	absent	absent	absent	absent	absent	absent	absent	absent
Fat involvement	present	present	present	present	present	present	present	present	present	present	present	present
Invading cartilage	absent	absent	absent	absent	absent	absent	absent	absent	absent	absent	absent	absent
Spindle morphology	absent	absent	absent	absent	absent	absent	absent	absent	absent	absent	absent	absent
Epithelioid morphology	present	present	present	present	present	present	present	present	present	present	present	present
Neural differentiation	absent	absent	absent	absent	absent	absent	absent	absent	absent	absent	absent	absent
Marked pigmentation	present	present	present	present	present	present	present	present	present	present	present	present
Mitoses per squared millimeter	0	0	0	0	0	0	0	0	0	0	0	0
Necrosis	absent	absent	absent	absent	absent	absent	absent	absent	absent	absent	absent	absent
Dermal hyalinization/fibrosis	absent	absent	absent	absent	absent	absent	absent	absent	absent	absent	absent	absent

Table S2: Gene Ontology (GO) analysis on CTC-enriched genes. (Related to Figure 3)

Top 10 functional Categories of CTC-enriched genes			
Functional Categories	Number of genes	Number of genes expected	P-Value
Lysosome	15	1.6	6.57×10^{-11}
Plasma membrane	62	29	1.18×10^{-09}
Inflammatory response	15	2.3	1.32×10^{-08}
Protein binding	104	67.1	1.67×10^{-08}
Extracellular region	40	16.6	1.22×10^{-07}
Immune response	15	3	3.66×10^{-07}
Signal transduction	30	11.3	7.70×10^{-07}
Cellular component movement	9	1	9.37×10^{-07}
External side of plasma membrane	10	1.4	1.42×10^{-06}
Melanosome	8	1	5.20×10^{-06}

Table S3: Selected list of CTC genes. (Related to Figure 3)

Supplemental Table 2: Selected list of genes expressed in CTCs		
Gene	Description	Function
Tgfbi	Transforming growth factor, beta induced	TGFbeta signaling
Mafb	V-maf musculoaponeurotic fibrosarcoma oncogene family, protein B (avian)	
Bak1	BCL2-antagonist/killer 1	
Api5	Apoptosis inhibitor 5	
Fn1	Fibronectin 1	EMT marker
Tgfb1	Transforming growth factor, beta 1	TGFbeta signaling
Zeb2	Zinc finger E-box binding homeobox 2	EMT inducer
Cd44	CD44 antigen	
Lyn	Yamaguchi sarcoma viral (v-yes-1) oncogene homolog	
Klf6	Kruppel-like factor 6	Stem cell differentiation, Klf family member
Vim	Vimentin	EMT marker
App	Amyloid beta (A4) precursor protein	
Klf4	Kruppel-like factor 4 (gut)	Stem cell reprogramming
Akt1	Thymoma viral proto-oncogene 1	
Arpc5	Actin related protein 2/3 complex, subunit 5	
Arpc2	Actin related protein 2/3 complex, subunit 2	
Ceacam1	Carcinoembryonic antigen-related cell adhesion molecule 1	CD66a membrane antigen
Sbno2	Strawberry notch homolog 2 (Drosophila)	Positive regulator of EGF/RAS
Hsp90b1	Heat shock protein 90, beta (Grp94), member 1	
Diap1	Diaphanous homolog 1 (Drosophila)	Microtubule rearrangement, Neuron migration
Zic1	Zinc finger protein of the cerebellum 1	
Wipf1	WAS/WASL interacting protein family, member 1	
Zyx	Zyxin	Tgfb induced cell movement
Rhoa	Ras homolog gene family, member A	Cell motility
Ssh2	Slingshot homolog 2 (Drosophila)	Actin dynamics
S100a6	S100 calcium binding protein A6 (calcyclin)	
Tgfbr1	Transforming growth factor, beta receptor I	
Neurl3	Neuralized homolog 3 homolog (Drosophila)	Notch signaling
Snord35a	small nucleolar RNA, C/D box 35A	
Snord33	small nucleolar RNA, C/D box 33	
Snora70	Small nucleolar RNA, H/ACA box 70	
Glipr2	GLI pathogenesis-related 2	Tgfb/SHH signaling pathway downstream
Akt2	Thymoma viral proto-oncogene 2	
Pum2	Pumilio 2 (Drosophila)	mRNA translation regulation
Hif1a	Hypoxia inducible factor 1, alpha subunit	Hypoxia
Tgfbr2	Transforming growth factor, beta receptor II	
Myc	Myelocytomatosis oncogene	
Fli1	Friend leukemia integration 1	ETS transcription factor
Itch	Itchy, E3 ubiquitin protein ligase	
Cic	Capicua homolog (Drosophila)	granule neuron development
Notch2	Notch gene homolog 2 (Drosophila)	Notch signaling
Brpf1	Bromodomain and PHD finger containing, 1	
Rock2	Rho-associated coiled-coil containing protein kinase 2	
Ets1	E26 avian leukemia oncogene 1, 5' domain	
Hsp90ab1	Heat shock protein 90 alpha (cytosolic), class B member 1	
Qk	Quaking	CNS development
Stat6	Signal transducer and activator of transcription 6	
Ezr	Ezrin	
Malat1	Metastasis associated lung adenocarcinoma transcript 1 (non-coding RNA)	Non-coding lincRNA
Tet2	Tet oncogene family member 2	
Vav1	Vav 1 oncogene	
Spnb2	Spectrin beta 2	
Stat3	Signal transducer and activator of transcription 3	
Jak1	Janus kinase 1	
Ewsr1	Ewing sarcoma breakpoint region 1	
Kdm2a	Lysine (K)-specific demethylase 2A	
Nras	Neuroblastoma ras oncogene	
Hsp90aa1	Heat shock protein 90, alpha (cytosolic), class A member 1	
Sbno1	Sno, strawberry notch homolog 1 (Drosophila)	
Kdm6b	KDM1 lysine (K)-specific demethylase 6B	
Pten	Phosphatase and tensin homolog	
Msi2	Musashi homolog 2 (Drosophila)	NSC, HSC proliferation/differentiation
Cnr1	Cannabinoid receptor 1 (brain)	
Sp1	Trans-acting transcription factor 1	
Msl2	Male-specific lethal 2 homolog (Drosophila)	
Klf2	Kruppel-like factor 2 (lung)	Klf family member

Table S4: List of antibodies used in melanoma patient CTC enrichment and identification. (Related to Figure 4)

Antibodies used for melanoma CTC capture			
Antigen	Clone	Isotype	Reference
CSPG4	LHM-2	Mouse IgG1	Kupsch et al. (1995)
Melanotransferrin/P97	L-235	Mouse IgG1	Houghton et al. (1982)
MCAM	P1H12	Mouse IgG1	Denton et al. (1992); Solovey et al. (1997)
CD117	104D2	Mouse IgG1	Ohashi et al. (1996) Rappold et al. (1997)
NGFR	NGFR5	Mouse IgG1	Boiko et al. (2010) Thompson et al. (1989)
N-Cadherin	8C11	Mouse IgG1	Puch et al. (2001)
EGFR	Certuximab	Chimeric	Hoek et al. (2008) Prewett et al. (1996)
EphA2		Goat polyclonal	Udayakumar et al. (2011)
CD90	5E10	Mouse IgG	Winnepenninckx et al. (2003)
c-Met		Goat polyclonal	Natali et al. (1993)
A2B5	105	Mouse IgM	Eisenbarth et al. (1979); Yamamura and Mishima (1990)
HNK-1	HNK-1	Mouse IgM	Schachner and Martini (1995); Tang et al. (1996)
Antibodies used for melanoma CTC detection by IF			
Antigen	Clone	Isotype	Reference
CSPG4	9.2.27	Mouse IgG2a	Morgan et al. (1981)
MCAM	SHM-57	Mouse IgG2a	
TYRP-1	TA99	Mouse IgG2a	Thomson et al. (1985)
alpha-SMA	1A4	Mouse IgG2a	Banerjee et al. (1996) Dundr et al. (2009) (Supplemental figure 1)

SUPPLEMENTAL REFERENCES

Banerjee, S. S., Bishop, P. W., Nicholson, C. M., and Eyden, B. P. (1996). Malignant melanoma showing smooth muscle differentiation. Journal of clinical pathology *49*, 950-951.

Boiko, A. D., Razorenova, O. V., van de Rijn, M., Swetter, S. M., Johnson, D. L., Ly, D. P., Butler, P. D., Yang, G. P., Joshua, B., Kaplan, M. J.*, et al.* (2010). Human melanoma-initiating cells express neural crest nerve growth factor receptor CD271. Nature *466*, 133-137.

Dankort, D., Curley, D. P., Cartlidge, R. A., Nelson, B., Karnezis, A. N., Damsky, W. E., Jr., You, M. J., DePinho, R. A., McMahon, M., and Bosenberg, M. (2009). Braf(V600E) cooperates with Pten loss to induce metastatic melanoma. Nat Genet *41*, 544-552.

Denton, K. J., Stretch, J. R., Gatter, K. C., and Harris, A. L. (1992). A study of adhesion molecules as markers of progression in malignant melanoma. J Pathol *167*, 187-191.

Dundr, P., Povysil, C., and Tvrdik, D. (2009). Actin expression in neural crest cell-derived tumors including schwannomas, malignant peripheral nerve sheath tumors, neurofibromas and melanocytic tumors. Pathol Int *59*, 86-90.

Eisenbarth, G. S., Walsh, F. S., and Nirenberg, M. (1979). Monoclonal antibody to a plasma membrane antigen of neurons. Proc Natl Acad Sci of U S A *76*, 4913-4917.

Hoek, K. S., Eichhoff, O. M., Schlegel, N. C., Dobbeling, U., Kobert, N., Schaerer, L., Hemmi, S., and Dummer, R. (2008). In vivo switching of human melanoma cells between proliferative and invasive states. Cancer Res *68*, 650-656.

Houghton, A. N., Eisinger, M., Albino, A. P., Cairncross, J. G., and Old, L. J. (1982). Surface antigens of melanocytes and melanomas. Markers of melanocyte differentiation and melanoma subsets. J Exp Med *156*, 1755-1766.

Kupsch, J. M., Tidman, N., Bishop, J. A., McKay, I., Leigh, I., and Crowe, J. S. (1995). Generation and selection of monoclonal antibodies, single-chain Fv and antibody fusion phage specific for human melanoma-associated antigens. Melanoma Res *5*, 403-411.

Morgan, A. C., Jr., Galloway, D. R., and Reisfeld, R. A. (1981). Production and characterization of monoclonal antibody to a melanoma specific glycoprotein. Hybridoma *1*, 27-36.

Natali, P. G., Nicotra, M. R., Di Renzo, M. F., Prat, M., Bigotti, A., Cavaliere, R., and Comoglio, P. M. (1993). Expression of the c-Met/HGF receptor in human melanocytic neoplasms: demonstration of the relationship to malignant melanoma tumour progression. Br J Cancer *68*, 746-750.

Ohashi, A., Funasaka, Y., Ueda, M., and Ichihashi, M. (1996). c-KIT receptor expression in cutaneous malignant melanoma and benign melanotic naevi. Melanoma Res *6*, 25-30.

Prewett, M., Rockwell, P., Rockwell, R. F., Giorgio, N. A., Mendelsohn, J., Scher, H. I., and Goldstein, N. I. (1996). The biologic effects of C225, a chimeric monoclonal antibody to the EGFR, on human prostate carcinoma. J Immunother Emphasis Tumor Immunol *19*, 419-427.

Puch, S., Armeanu, S., Kibler, C., Johnson, K. R., Muller, C. A., Wheelock, M. J., and Klein, G. (2001). N-cadherin is developmentally regulated and functionally involved in early hematopoietic cell differentiation. J Cell Sci *114*, 1567-1577.

Rappold, I., Ziegler, B. L., Kohler, I., Marchetto, S., Rosnet, O., Birnbaum, D., Simmons, P. J., Zannettino, A. C., Hill, B., Neu, S.*, et al.* (1997). Functional and phenotypic

characterization of cord blood and bone marrow subsets expressing FLT3 (CD135) receptor tyrosine kinase. Blood *90*, 111-125.
Schachner, M., and Martini, R. (1995). Glycans and the modulation of neural-recognition molecule function. Trends Neurosci *18*, 183-191.
Solovey, A., Lin, Y., Browne, P., Choong, S., Wayner, E., and Hebbel, R. P. (1997). Circulating activated endothelial cells in sickle cell anemia. N Engl J Med *337*, 1584-1590.
Stott, S. L., Hsu, C. H., Tsukrov, D. I., Yu, M., Miyamoto, D. T., Waltman, B. A., Rothenberg, S. M., Shah, A. M., Smas, M. E., Korir, G. K.*, et al.* (2010). Isolation of circulating tumor cells using a microvortex-generating herringbone-chip. Proc Natl Acad Sci U S A *107*, 18392-18397.
Tang, N. E., Luyten, G. P., Mooy, C. M., Naus, N. C., de Jong, P. T., and Luider, T. M. (1996). HNK-1 antigens on uveal and cutaneous melanoma cell lines. Melanoma Res *6*, 411-418.
Thompson, S. J., Schatteman, G. C., Gown, A. M., and Bothwell, M. (1989). A monoclonal antibody against nerve growth factor receptor. Immunohistochemical analysis of normal and neoplastic human tissue. Am J Clin Pathol *92*, 415-423.
Thomson, T. M., Mattes, M. J., Roux, L., Old, L. J., and Lloyd, K. O. (1985). Pigmentation-associated glycoprotein of human melanomas and melanocytes: definition with a mouse monoclonal antibody. J Invest Dermatol *85*, 169-174.
Udayakumar, D., Zhang, G., Ji, Z., Njauw, C. N., Mroz, P., and Tsao, H. (2011). EphA2 is a critical oncogene in melanoma. Oncogene *30*, 4921-4929.
Winnepenninckx, V., De Vos, R., Stas, M., and van den Oord, J. J. (2003). New phenotypical and ultrastructural findings in spindle cell (desmoplastic/neurotropic) melanoma. Appl Immunohistochem Mol Morphol *11*, 319-325.
Yamamura, K., and Mishima, Y. (1990). Antigen dynamics in melanocytic and nevocytic melanoma oncogenesis: anti-ganglioside and anti-ras p21 antibodies as markers of tumor progression. J Invest Dermatol *94*, 174-182.
Yu, M., Ting, D. T., Stott, S. L., Wittner, B. S., Ozsolak, F., Paul, S., Ciciliano, J. C., Smas, M. E., Winokur, D., Gilman, A. J.*, et al.* (2012). RNA sequencing of pancreatic circulating tumour cells implicates WNT signalling in metastasis. Nature *487*, 510-513.